

NEW ENERGY SOURCE CONTROLLED BY GRAVITY ALONE?

Reva Kay Williams

Department of Astronomy, University of Florida, Gainesville, FL 32611

revak@astro.ufl.edu

ABSTRACT

In this paper, I present a theoretical and numerical (Monte Carlo) *N-particle* fully relativistic 4-D analysis of Penrose scattering processes (Compton and $\gamma\gamma \rightarrow e^-e^+$) in the ergosphere of a supermassive Kerr (rotating) black hole. These general relativistic model calculations surprisingly reveal that the observed high energies and luminosities of quasars and other active galactic nuclei, the collimated jets about the polar axis, and the asymmetrical jets (which can be enhanced by relativistic Doppler beaming effects) *all* are inherent properties of rotating black holes. From this analysis, it is shown that the Penrose scattered escaping relativistic particles exhibit tightly wound coil-like cone distributions (highly collimated vortical jet distributions) about the polar axis, with helical polar angles of escape varying from 0.5° to 30° for the highest energy particles. It is also shown that the gravitomagnetic (GM) field, which causes the dragging of inertial frames, exerts a force acting on the momentum vectors of the incident and scattered particles, causing the particle emission to be asymmetrical above and below the equatorial plane, thus appearing to break the equatorial reflection symmetry of the Kerr metric. When the accretion disk is assumed to be a two-temperature bistable thin disk/ion corona (or torus \equiv advection-dominated accretion flow), energies as high as 54 GeV can be attained by these Penrose processes alone; and when relativistic beaming is included, energies in the TeV range can be achieved, agreeing with observations of some BL Lac objects. When this model is applied specifically to quasars 3C 279 and 3C 273, and the Seyfert 1 galaxy MCG—60-30-15, their observed high energy luminosity spectra can be duplicated and explained. This energy-momentum extraction model can be applied to any size black hole, irrespective of the mass, and therefore applies to microquasars as well. When applied to the classical galactic black hole source Cygnus X-1, the results are consistent with observations. The consistency of these Penrose model calculations with observations suggests that the external magnetic field of the accretion disk plays a negligible role in the extraction of energy-momentum from a rotating black hole, inside the ergosphere, close to the event horizon, where gravitational forces, and thus the dynamics of the black hole, appear to be dominant, as would be expected.

Subject headings: acceleration of particles—black hole physics—galaxies: jets—quasars: general—gravitation—relativity

1. Introduction

For almost four decades, since the discovery of quasars, mounting observational evidence has accumulated that black holes indeed exist in nature. Recent observations (Wilms et al. 2001) of the steep emissivity of Seyfert 1 galaxy MCG—60-30-15, indicating strong photon emission at radii near the event horizon; and observations of the lack of evidence of the expected ion “dusty” torus of M87 (Perlman et al. 2001), have prompted astrophysicists to suggest a new energy source. However, it is hardly a new energy source to relativists, i.e., those who study Einstein’s Theory of General Relativity. They knew for sometime, at least theoretically, what black holes were capable of doing (Williams 1991, 1995). Williams (1995, 2002a, 20002b) has shown, through theoretical and numerical (Monte Carlo) *N-particle* calculations of Penrose (1969) processes, occurring at radii inside the ergosphere of a rotating black hole near the event horizon: including the “plunging” regimes (Bardeen, Press, & Teukolsky 1972), that the black hole can yield escaping particles with energies up to ~ 54 GeV. These particles escape in the form of collimated, symmetrical and asymmetrical, jets about the polar axis, confirming the existence of intrinsically collimated vortical jets, found theoretical by de Felice & Calvani (1972); de Felice & Curir (1992); de Felice & Carlotto (1997); de Felice & Zanotti (2000): from geometrical studies of particle trajectories in a Kerr (1963) metric (which in general describes the spacetime separation of events in the gravitational field of a rotating compact massive object).

In light of these new observational surprises (of the above black hole sources), particularly the steep emissivity of X-rays producing the broad Fe K α emission line at ~ 6 keV in MCG—6-30-15 (Wilms et al. 2001) and similar AGNs, it appears that gravity has won over proposed forms of electromagnetic energy extraction from a black hole, as will be described in this paper. This should be of no surprise near the event horizon, where the gravitational forces are so strong that electromagnetic radiation itself becomes trapped.

Overall, energy extraction from black holes and the production of their associated jets have been the most poorly understood phenomena of today. It is clear that gravitational accretion and magnetic fields play a role, but how? has been the mystery. We observe these jets in quasars and microquasars due to supermassive and stellar size black holes, respectively. Therefore, we know that any effective model must have the commonality to explain jets in both systems. At present there are two popular trains of thought associated with energy extraction and the production of jets in black holes: one is that the jets are inherent properties of geodesic trajectories in the Kerr metric of a rotating black hole, and thus, can be described by Einstein’s general theory of relativity; and the other is that the accretion disk and its magnetic field through magnetohydrodynamics (MHD) are producing the jets. Perhaps it could be a combination of the two, with gravity controlling the flow near the event horizon, and MHD controlling the flow at distances farther away. The observations of the jet of M87 suggest this may be the case (Junor, Biretta, & Livio 1999; Perlman et al. 2001).

There are some proposed MHD model calculations using a general relativistic accretion disk, that involve having the magnetic field lines of the disk “anchor” to conductive ionized particles of

the disk, inside the ergospheric region, extracting rotational energy from a Kerr black hole, by way of a Poynting flux of electromagnetic energy, out to infinity. Such models have been proposed to explain recent observations of possible direct evidence for the extraction of energy from a rotating black hole (Wilms et al. 2001). In this paper, however, I point out problems with such models that make these models highly improbable to be at work, i.e., extracting the energy needed to be consistent with general observations of sources powered by black holes. It is agreed by the author that some form of the Penrose mechanism is employed, but it is argued below that electromagnetic energy extraction is not an effective way to use this mechanism. Associated problems with such models are described in the Appendix.

In a classical paper by Bardeen et al. (1972), astrophysical implausible Penrose processes are discussed concerning the breakup of subrelativistic objects in the ergosphere. However, I point out that the “Penrose-Williams” mechanism, described by Williams (1995), involves relativistic scattering processes: such processes can be very efficient (Piran, Shaham, & Katz 1975; Williams 1995), and do not fall under the category of being implausible due to hydrodynamical constraints (Bardeen et al. 1972), i.e., since the incident and target particles in the collisions are already relativistic, having speeds $\sim c$.

The Penrose mechanism as described here (Williams 1995) has a “one-on-one” consistent relationship with accretion disk particles: for example, particles from the accretion disk can populate the high energy gravitationally blueshifted trapped orbits (or plunging orbits, i.e., trapped orbits with $E/\mu_o \geq 1$), at $r < r_{\text{ms}}$. Particles in these now populated orbits can undergo Penrose processes with lower soft X-ray energy infalling accretion disk photons: Penrose Compton scattering (PCS) produces copious distributions of high energy X-rays and soft γ -rays, and Penrose pair production (PPP) ($\gamma\gamma \rightarrow e^-e^+$) produces copious distributions of relativistic e^-e^+ pairs, with up to $\sim 90\%$ of the particles escaping along vortical-like orbits that circle the polar axis of the KBH many times, as spacetime itself is dragged around: due to gravity. The particles escape to infinity along well defined four-momentum trajectories, some that intersect the disk (i.e., returning to be reprocessed and/or escaping to infinity). This scenario is particularly consistent with recent observations of MCG—6-30-15 (§ 3.4.2), and other black hole sources (§ 3.4).

Importantly, in these Penrose processes we do not need the magnetic field of the accretion disk to “communicate” between the accretion disk and the black hole. Therefore, there is no need for the Blandford and Znajek (BZ) (1977) proposed type models (and their many associated problems) in the direct role of energy extraction from a spinning black hole. However, their presence appears to be need once particles are on escaping orbits, serving the same effects they do in the jets of protostars, i.e., appearing to have a dominant role on a large scale, within the weak field limit, at distances outside the strong effects of general relativity.

As for producing the observed synchrotron radiation indicating the present of a magnetic field near the core region, it could very well be produced by the intrinsically self-induced magnetic field due to the dynamo-like action of the escaping Penrose produced e^-e^+ pairs, escaping on vortical,

coil-like trajectories concentric the polar axis, in the form of a swirling “current” plasma. This, therefore, adds more to the unimportance of the accretion disk magnetic field near the event horizon.

Moreover, although suggested to be evidence of rotational magnetic energy extraction from the Seyfert 1 galaxy MCG—60-30-15 (Wilms et al. 2001), it appears, as we shall see in this paper, that it is gravitational energy-momentum being extracted, in the form of a relativistic particle flux via Penrose processes, as described by Williams (1995), and *not* the Poynting flux of electromagnetic energy suggested: produced by magnetic field lines torquing the black hole or plunging accretion disk material, as described by the BZ-type models. In the Penrose-Williams mechanism, the steep emissivity profile [$\varepsilon(r) \sim r^{-5}$] of X-ray photons observed (Wilms et al. 2001), requiring a X-ray source that is both powerful and very centrally concentrated (which cannot be explained by standard accretion disk models), is consistent with energy being extracted by Penrose Compton scattering processes, occurring at radii between the marginally bound and marginally stable orbits, r_{mb} and r_{ms} , respectively (Williams 1995). This black hole source MCG—60-30-15 will be discussed further in § 3.4.2.

Nevertheless, once these Penrose processes have occurred and particles are on escaping trajectories, they can then interact, say with the expected large scale structure disk magnetic field: at some effective radius r where this field becomes important in jet collimation, probably similar to relative radii of collimated bi-polar jets of protostars, which, as mentioned above, appear to be undergoing some type of BZ effect—the direct effect is still somewhat unclear. It appears that the magnetic field of the accretion disk serves to aid in collimating into jets gravitational binding energy release due to gravitational accretion, in both protostars and AGNs (or microquasars); however, in the latter the jets are superimposed with collimated particles from Penrose processes.

So, overall, in this paper, an analysis of the Penrose mechanism is presented to describe gravitational-particle interactions close to the event horizon at radii $< r_{\text{ms}} \simeq 1.2M$, the marginal stable orbit, and inward to the *photon orbit*, $r_{\text{ph}} \simeq 1.074M$, for a canonical KBH with $a = 0.998M$ (Thorne 1974), where a is the angular momentum per unit mass parameter. In this fully general relativistic description, polar jets of relativistic particles of photons and electron-positron (e^-e^+) pairs are produced and collimated by gravity alone, without the necessity of the external magnetic field of the accretion disk. This theoretical and numerical model of Penrose processes can apply to any size black hole, and suggests a complete theory for the extraction of energy-momentum from a rotating black hole. In § 2 a summary of the general formalism of the model is presented. In § 3, results of theoretical and numerical calculated luminosities and energies are presented, along with discussion of the escaping particles’ space momentum trajectories: featuring asymmetrical polar distributions and vortical orbits. Also in § 3, agreement with observations of specific sources are presented. Finally, in § 4 a summary and conclusions are presented.

2. Model Formalism

The primary model (Williams 1995) consists of a supermassive $10^8 M_\odot$ rotating Kerr black hole plus particles from an assumed relativistic bistable thin disk/ion corona [or torus \equiv advection-dominated accretion flow (ADAF): two-temperature [separate temperatures for protons ($\sim 10^{12}$ K) and electrons ($\sim 10^9$ K)] accretion flow. The bistable accretion disk can exist either in the thin disk phase and/or the ion corona (or ADAF) phase, or oscillate between the two (see Williams 2002a and references therein) in various degrees—which could be responsible for the observed variability. The Penrose effect as employed here can operate in either phase. The Penrose mechanism is used to extract rotational energy-momentum by scattering processes inside the ergosphere ($r_0 \simeq 2M$, in the equatorial plane for $a = 0.998M$). See Williams (1995) for a detailed description of the model. The “quasi-Penrose” (Williams 1991, 1995) processes investigated are (a) Penrose Compton scattering (PCS) of equatorial low energy radially infalling photons by equatorially confined ($Q_e = 0$) and nonequatorially confined ($Q_e \neq 0$) orbiting target electrons, at radii between the marginally bound ($r_{mb} \simeq 1.089M$) and marginally stable ($r_{ms} \simeq 1.2M$) orbits, where Q_e is the so-called Carter constant (Carter 1968), referred to as the Q value (Williams 1995); (b) Penrose pair production (PPP) ($\gamma p \rightarrow e^- e^+ p$) at r_{mb} ; and (c) PPP ($\gamma\gamma \rightarrow e^- e^+$) by equatorial low energy radially infalling photons and high energy gravitationally blueshifted (by factor $e^{-\nu} \simeq 52.3$) nonequatorially confined γ -rays at the photon orbit ($r_{ph} \simeq 1.074M$), where $e^{-\nu}$ is the “blueshift” factor given by the g_{tt} component of the Kerr metric (see Williams 1995). Although in the scattering plane the incident angle of the infalling photon relative to the target particle is expected in general to be at least between $0^\circ - 90^\circ$ (due to the bending of light and/or inertial frame dragging), maximum energy is extracted in the process when the incident angle is 90° , as it is for radially infalling photons ($L = P_\Phi = 0$, where L is the azimuthal coordinate angular momentum). Note, the target particles are initially in bound (marginally stable or unstable) trapped orbits, trapped in the sense of possibly having no other way of escaping save these Penrose processes (Bardeen et al. 1972; Williams 1995). Note also that, as the nonequatorially confined target particle, whose orbital trajectory is derived by Williams (1991, 1995; see also Williams 2002b), passes through the equatorial plane, in its bound circular orbit at constant radius, the Q value, a constant of motion as measured by an observer at infinity (Carter 1968; Williams 1995), equals P_Θ^2 , where P_Θ is the polar coordinate momentum of the particle. Setting $P_\Theta = 0$, in the Carter constant expression for the orbital Q value, gives the maximum and minimum latitudinal angles of the trajectories about the equatorial plane for Wilkins’ (1972) “spherical-like” nonequatorially confined orbits (see Williams 2002a). These unstable, bound or marginally bound orbits (equatorial, nonequatorial) of the target particles are assumed to be populated by accretion disk instability processes and prior Penrose processes. Such particles must satisfy conditions to have a turning point at the scattering radius (note, a bound stable orbit is considered to have a “perpetual” turning point). These conditions depend on the orbital conserved parameters of the particle: E , the energy, and L , or Q . In Williams (1995, 2002b) such conditions are discussed in details; see also the possible scenario discussion in § 3.2 of this present manuscript. In addition, the “instability phase” during which the target particle orbits are presumed to be populated could very well be related to the

timescale of the prominent observed variabilities of the source.

Radial infalling equatorially confined incident photons are assumed, again for maximum energy extraction, and for more effective scattering, since it appears that an infalling equatorially confined photon will not acquire gravitationally blueshifted orbital energy as measured by an observer at infinity, only frame dragging blueshifted energy. This is because the Q value of such photons is zero [see eq. (2.27) of Williams (1995)]. The incoming photons, however, need not be confined to the equatorial plane. In these calculations if equatorially confined infalling photons were not desired, $\sqrt{Q_{\text{ph}}} \equiv (P_{\text{ph}})_{\Theta}$ of the initial photon would not be set equal zero. That is, the model calculation is set up such that one can change the initial energy-momentum four vector components (or four-momenta) of the incident and target particles to accommodate any 3-space dimensional geometrical disk configuration. Moreover, in an ADAF (including the ion corona), during the infall of particles, through the ergosphere, some of the particles are expected to become trapped in nonequatorial “spherical-like orbits” (Wilkins 1972): such orbits would pass through the equatorial plane: here is where the scattering takes place in these calculations. Note, the target photons at the photon orbit can only exist in nonequatorially confined orbits (Williams 1995); this is also pointed out by Bardeen (1973).

Monte Carlo N -particle computer simulations of up to $\sim 70,000$ scattering events of infalling accretion disk photons (normalized to a power-law distribution) are executed for each computed Penrose produced luminosity spectrum (Williams 2002a). Energy and momentum (i.e., four-momentum) spectra of escaping particles (γ -rays, e^-e^+ pairs), as measured by an observer at infinity, are obtained per each 2000 scattering events per monochromatic infalling photon distribution. The following constituents are used (Williams 1995): (1) General relativity is used [the Kerr metric spacetime geometry yields equatorially and nonequatorially confined spherical-like (Wilkins 1972) particle orbits and escape conditions, conserved energy and angular momentum parameters, and transformations from the Boyer-Lindquist coordinate frame (BLF) to the local nonrotating frame (LNRF)]. Note, BLF is the observer at infinity (Boyer & Lindquist 1967); LNRF is the local Minkowski (flat) spacetime. (2) Special relativity is used [in the LNRF, physical processes (i.e., the scatterings) are done; Lorentz transformations between inertial frames are performed; and Lorentz invariant laws are applied]. (3) Cross sections are used [application of the Monte Carlo method to the cross sections, in the electron rest frame for PCS, in the proton rest frame for $\text{PPP}(\gamma p \rightarrow e^-e^+p)$, and in the center of momentum frame for $\text{PPP}(\gamma\gamma \rightarrow e^-e^+)$, give the distributions of scattering angles and final energies].

3. Overall Results and Discussion

3.1. Energy and Luminosity Spectra Extracted

In general, energies attained consistent with the proposed accretion disk model are the following (Williams 1995):

I. *PCS*.—For the input photon energy range ~ 5 eV to 0.15 MeV, the corresponding output energy range is ~ 3 keV to 7 MeV. The input photon range covers the range of photons in a thin disk (~ 5 eV, $\sim 0.511 - 3.5$ keV), thin disk/ion corona (~ 5 eV, $\sim 0.511 - 3.5$ keV, $\sim 30 - 150$ keV), and ADAF ($\sim 30 - 150$ keV) for a $10^8 M_\odot$ KBH (Williams 2002a, 1995). The input luminosity spectra are based on observations, consistent with a power-law distribution in the X-ray, and accretion disk theory. Typical output luminosity spectral distributions from PCS are displayed in Figure 1a: the curves passing through numbers 1 – 13 (as will be described below in the discussion of the model produced luminosity). Note, the \sim eV input photons are presumed to come, in general, from a relatively cooler region of the disk, say the “middle” region of the classical thin accretion disk—as defined by Novikov & Thorne (1973), or even the “inner” region during say a phase of relatively low accretion rate.

II. *PPP* ($\gamma p \rightarrow e^- e^+ p$).—There are no escaping pairs for radially infalling equatorially confined γ -rays (~ 40 MeV) and no energy boost: implying that the assumption: negligible recoil energy given to the proton, made in the conventional cross section, and perhaps the geometry of the scattering must be modified. It had been predicted (Leiter & Kafatos 1978) that pairs with energies (~ 1 GeV) could escape. See Williams (1995) for further details of this PPP process.

III. *PPP* ($\gamma\gamma \rightarrow e^- e^+$).—For input photon energy range ~ 3.5 keV to 200 MeV, yields output ($e^- e^+$) energy range ~ 1 MeV to 10 GeV (for MB), and higher up to ~ 54 GeV (for PL, with input photon energy ~ 2 GeV), where MB and PL \equiv Maxwell-Boltzmann and power-law distributions, respectively, for the accretion disk protons: undergoing nuclear proton-proton scatterings, which yield neutral pion decays $\pi^0 \rightarrow \gamma\gamma$ (Eilek 1980; Eilek & Kafatos 1983; Mahadevan, Narayan, & Krolik 1997), to populate the photon orbit. Below, I refer to such decays and subsequent $e^- e^+$ pair production (from the resultant photons), which can occur in ADAFs, as Eilek’s particles (Eilek 1980).

Specific disk model correlations are the following [see Williams (1995, 2002a) for further details]:

1. Without instabilities [\Rightarrow the classical thin disk (Novikov & Thorne 1973)]:

- a) PCS can convert infalling (incident) soft X-rays $0.511 - 3.5$ keV to moderate X-rays, escaping with energies in the range $\sim 3 - 262$ keV. The upper and lower bounds on the energy of the outgoing photons are set by the initial four-momentum conditions of the target orbiting electron (with $E_e \simeq 0.539$ MeV) and the incident photon (with $E_{\text{ph}} = 0.511 - 3.5$ keV) undergoing PCS. These initial four-momenta are consistent in general with the following: theoretical accretion disk models, the threshold energy values for the scattering process to occur, and what brings about the most “efficient” energy extraction process [see Williams (1995) for details defining the efficiencies]. These momenta are substituted into appropriate theoretical analytically derived model equations (describing the Penrose scattering process in the ergosphere of a Kerr black hole; see Williams 1995), and these equations are computed. The output energy range presented above gives the lowest and highest energy values obtained

by the escaping Penrose Compton scattered (PCS) photons, for the given input energy range of the incident photons.

- b) Inwardly directed PCS photons that have an appropriate turning point (see Williams 2002b) can serve as seed γ -rays for the PPP ($\gamma\gamma \rightarrow e^-e^+$) at the photon orbit. Specifically, the PCS photons that satisfy conditions to have a turning point, acquire blueshifted energies as high as ~ 7 MeV.
- c) PPP ($\gamma\gamma \rightarrow e^-e^+$) can convert infalling soft X-ray photons to relativistic e^-e^+ pairs, escaping with energies in the range ~ 2 –6 MeV, i.e., infalling photons can pair produce at the photon orbit with photons populated by prior PCS.

2. With instabilities (\Rightarrow the thin disk/ion corona or ADAF):

- a) PCS can convert infalling X-rays 0.03–0.15 MeV to escaping photon energies in the range ~ 0.4 –7 MeV. The differences in the calculations of the above case in item 1 and the present case of item 2 are the energies of the infalling incident photons and the target electrons ($E_e \simeq 0.539$ –4.8 MeV), including nonequatorially confined targets: $\pm 1.68Mm_e \leq (P_e)_\Theta \equiv \sqrt{Q_e} \leq \pm 10.05Mm_e$ for $0.963 \text{ MeV} \lesssim E_e \lesssim 4.8 \text{ MeV}$, corresponding to ADAFs with $30 \text{ keV} \lesssim kT_e \lesssim 150 \text{ keV}$, respectively, where $(P_e)_\Theta$ is the polar coordinate momentum component as measured by an observer at infinity (i.e., in the BLF; see § 2). [Note, the conserved energy $E = E(Q)$ and azimuthal angular momentum $L = L(Q)$ of the nonequatorially confined test particle orbits are given by analytically derived expressions presented in Williams (2002b, 1995).] The accretion disk model, used, is discussed in details in Williams (2002a; see Figure 1 and Table 1 of that reference). In general, the target electron orbits are assumed to be populated during instability phases, more or less, in both the thin disk and thin disk/ion corona (or ADAF). In § 3.2 in the discussion of a possible scenario for “jet reversal,” a brief description is included on populating the target electron orbits from the inner region of a thin disk (Novikov & Thorne 1973).
- b) PCS photons that can populate the photon orbit (as in item 1.b) have blueshifted energies specifically in the range 27 – 57 MeV $\lesssim E''_{\text{ph}} \lesssim 348$ MeV, where E''_{ph} is the energy at the photon orbit due to prior PCS (Williams 2002b). The lower limits of E''_{ph} are due to PCS by equatorially [$E_e \simeq 0.539$ MeV, $(P_e)_\Theta = 0$], and nonequatorially [$E_e \simeq 0.96$ MeV, $(P_e)_\Theta = \pm 1.68Mm_e$] confined electron targets, respectively: note, these nonequatorially confined targets are assumed to come from an ADAF ($kT_e \sim 30$ keV).
- c) PPP ($\gamma\gamma \rightarrow e^-e^+$) can convert infalling soft X-ray photons to relativistic e^-e^+ pairs, escaping with energies in the range 26 – 56 $\lesssim E_{\mp} \lesssim 340$ MeV. Note, the stability of a turning point being perpetual (i.e., bound) at the photon orbit decreases with increasing energy of the incoming incident photons undergoing PCS by equatorially confined target electrons. These calculations show that the most stable orbits (or turning points) appear to be the ones in

which the infalling incident photons and the orbiting target electrons are self-consistent, i.e., of the same accretion disk phase (e.g., thin disk or ADAF).

Note, whenever the thin disk is present, the processes described above in items 2.*a*–2.*c* will occur in addition to those described in items 1.*a*–1.*c*.

3. With instabilities [⇒ the thin disk/ion corona model or ADAF plus Eilek’s particles (Eilek 1980; Eilek & Kafatos 1983) to populate the target particle orbits—of electrons and photons, particularly the large Q -value orbits; see Williams (1995)]:

- a)* PCS can convert infalling photons 5 eV–0.15 MeV to escaping energies in the range \sim 5 keV–7 MeV. That is, in addition to the energy distribution of escaping PCS photons given in item 2.*a*, the \sim 5 eV infalling photons, mentioned above in item I, might be important in this case. Eilek’s particles contribute to the ion corona, nonequatorially confined e^-e^+ pairs with energies peak around $E \sim 35$ MeV. At the peak, such electrons with inward trajectories ($P_r < 0$) might satisfy conditions to have a turning point at $r_{\text{mb}} < r < r_{\text{ms}}$ (Williams 2003), requiring $\sqrt{Q} \gtrsim 73Mm_e$, $\gtrsim 141Mm_e$ and/or $L \gtrsim 141Mm_e$, $\gtrsim 138Mm_e$, for the scattering radii r_{mb} , r_{ms} , respectively. If such electrons satisfy conditions to have a turning point, for example at r_{mb} , the PCS, of initial UV photons (\sim 5 eV), can produce escaping photons peaking in luminosity at $E'_{\text{ph}} \sim 2$ MeV, in the form of symmetrical polar jets (see § 3.2). This particular PCS could possibly be important under certain circumstances (see description below). [In addition, Eilek’s electrons may be an important source of synchrotron emission into the IR, for a magnetic field strength $B \sim 10^2$ gauss (see § 3.2) and/or important in conventional inverse Compton scattering of UV photons (\sim 5 eV) into the soft X-ray regime (\sim 24 keV).] The absolute efficiency ϵ_{abs} (\sim 0.03; see Williams 1995) is an order of magnitude larger for PCS involving UV photons and Eilek’s nonequatorially confined e^-e^+ pairs ($E_e \sim 35$ MeV), than for PCS involving UV photons and “normal” ion corona (or ADAF) electrons ($E_e \sim 4.8$ MeV), where we are assuming that these electron energies and momenta are consistent with that needed to populate the nonequatorially confined target electron orbits (see the scenario given in § 3.2; see also Williams 2003). For completion, PCS of UV (\sim 5 eV) thin disk photons by orbiting gravitationally blueshifted electron targets: $E_e \sim 4.8$ MeV, $\sqrt{Q_e} \sim 10Mm_e$, at r_{mb} : from the ion corona ($kT_e \sim 0.15$ MeV), produces escaping jet-like X-ray photons with energies \sim 5 – 28 keV, peaking in luminosity at $E'_{\text{ph}} \sim 28$ keV; this too may be important under certain circumstances, described as follows. An evolved radio loud quasar possessing a hot ion corona (with past sufficient Eilek’s particle nuclear reactions, however, lacking sufficient internal cooling) surrounding the region of a thin “cooler” UV inner disk [for a $10^8 M_\odot$ canonical KBH, viscosity $\alpha \sim 0.1$, mass accretion rate $\dot{M} \sim 10^{-4} M_\odot \text{ yr}^{-1}$ (Novikov and Thorne 1973; Williams 2002a)] might provide the necessary environment (i.e., circumstances) for such processes, described above, to occur, and be of importance. Note, PCS by Eilek’s nonequatorially confined e^-e^+ pairs \sim 6 – 12 MeV appears also to be important; these are discussed elsewhere (see Williams 2002a).

b) PPP ($\gamma\gamma \rightarrow e^-e^+$) can convert infalling soft X-rays to relativistic e^-e^+ pairs, escaping with energies ranging from ~ 300 MeV to as high as ~ 10 GeV [for MB (see item III above)], with input photon energy $\sim 6 - 200$ MeV from π^0 decays (Eilek & Kafatos 1983). That is, the input (target) photons are gravitationally blueshifted at photons orbit to energies $E_{\gamma 2} \sim 312$ MeV – 11 GeV, and are assumed to have a turning point at (or near) this scattering radius, with $\sqrt{Q_{\gamma 2}} \sim 9 - 312Mm_e$, respectively, where the subscript $\gamma 2$ represents the orbiting target photon. These PPP ($\gamma\gamma \rightarrow e^-e^+$) processes occur in addition to those given in item 2.c. The exact range of the PPP electrons will depend on which of the inwardly directed photons, after being blueshifted, satisfy conditions to have a turning point at or near the photon orbit [see Williams (2002b) for details]

Note that, there will be a slight time delay between PCS and PPP ($\gamma\gamma \rightarrow e^-e^+$) in items 1.a–1.c and 2.a–2.c, similar to the time offset (~ 5 min) X-ray and IR flares observed in microquasar GRS 1915+105, indicating that these flares are produced by the same event: The X-ray flares occur with the apparent disappearance of the inner X-ray emitting region of the accretion disk; and the subsequent IR flares are proposed to be due to synchrotron emitting ejecta of relativistic plasma into the polar direction (Eikenberry et al. 1999a; Eikenberry et al. 1999b).

Before discussing the luminosity spectra produced by these Penrose processes, we first discuss the “characteristic voids,” existing, in general, in observed spectra of all AGNs, more or less (compare Fig. 1a), and how these Penrose processes suggest an explanation for them. These observed voids appear to be caused by the “transitional energy regime” between thin disk ($E \sim 0.511 - 3.5$ keV) and ion corona (or ADAF) ($E \sim 30 - 150$ keV) states: therefore, we expect the Penrose process to be void of participating particles with energy in the range $3.5 \text{ keV} < E < 30 \text{ keV}$, i.e., if we assume such particles are sufficiently short-lived, save the disk electrons with $E \sim 17$ keV that can populate the equatorially confined target electron orbits at radii $r \sim r_{\text{mb}}$ (see § 3.2), where $E \equiv E_e \sim E_{\text{ph}}$ indicates a general particle energy, predicted theoretically by a particular phase of the accretion disk. The PCS photon energies E'_{ph} produced by incident and target particles in the transitional energy regime, and the subsequent gravitationally blueshifted energy E''_{ph} at the photon orbit, of incoming PCS photons satisfying conditions to have a turning point there (Williams 2002b), are found to give characteristic voids in the following regimes:

- (a) For thin disk/ion corona ($kT_e \sim 30$ keV): $0.262 \text{ MeV} < (E'_{\text{ph}})_{\text{void}} < 1.1 \text{ MeV}$ and $7.3 \text{ MeV} < (E''_{\text{ph}})_{\text{void}} < 57 \text{ MeV}$, where the upper limit originates from nonequatorially confined target electrons, consistent with the electron temperature in the ion corona (see Williams 2002a). Compare with item 2.b above.
- (b) For thin disk/ion corona ($kT_e \sim 50$ keV): $0.262 \text{ MeV} < (E'_{\text{ph}})_{\text{void}} < 2.1 \text{ MeV}$ and $7.3 \text{ MeV} < (E''_{\text{ph}})_{\text{void}} < 107 \text{ MeV}$.
- (c) For thin disk/ion corona ($kT_e \sim 150$ keV): $0.262 \text{ MeV} < (E'_{\text{ph}})_{\text{void}} < 5.3 \text{ MeV}$ and $7.3 \text{ MeV} < (E''_{\text{ph}})_{\text{void}} < 273 \text{ MeV}$.

Note, the PCS processes considered above are those occurring at or near r_{mb} : since the highest energy will be extracted from this scattering radius, and it appears that the orbits at this radius will be the first to be populated, as the disk temperature increases (§ 3.2), i.e., because of the larger blueshift factor acquired, and smaller Q_e needed, relative to these parameters at r_{ms} . The disk electrons energies $\gtrsim 30$ keV but $< \mu_e$, being blueshifted by a factor $e^{-\nu} \sim 32$ (see § 2), satisfying appropriate turning point conditions (Williams 2003), with $Q_e > 0$, are assumed to populate the nonequatorially confined target particle orbits for PCS (see also § 3.2), where $\mu_e \simeq 0.511$ MeV is the rest mass energy of an electron. A relativistic four-momentum treatment of disk particle, heating processes in thin disk/ion corona accretion, inside the ergosphere, appears to be needed to theoretically validate this plausible assumption: at present, however, we do not have such a model; therefore, we must rely on what observations convey to us.

Moreover, PCS by equatorially confined electron targets ($Q_e = 0$), assuming to originate from “mild” instabilities in the thin disk (that would cause the electron energy to increase to ~ 17 keV, however, while still predominantly in the thin disk phase) and radially infalling photons along the equatorial plane, originating from the ion corona, are not included in the above consideration of the characteristic voids. The reason is that observations suggest that such PCS may not be important (compare Fig. 1a, and curve between points 6 and 7). Further, for the subsequent gravitationally blueshift of such inward directed PCS photons, with $E'_{\text{ph}} \sim 0.51$ MeV, ~ 0.65 MeV, ~ 1.6 MeV, corresponding to potential turning point energies: $E''_{\text{ph}} \sim 27$ MeV, ~ 34 MeV, ~ 51 MeV, at the photon orbit, for the ion coronas in items (a)–(c), respectively, we find that most of these potential turning points, it seems, are “highly” uncertain. Nevertheless, as the energy of the target electron is increased ($Q_e \neq 0$), consistent with the general ion corona electron temperature, the uncertainty of the turning point orbit, being true, decreases.

Finally, in the above characteristic voids, PCS involving thin disks with energies less than $E \sim 3.5$ keV, and PCS involving Eilek’s nonequatorially confined e^-e^+ pairs, possibly occurring in the ion corona or ADAF (particularly $\sim 6 - 12$ MeV), are not included. Inclusion of these would slightly affect the voids, yet the distinctive characteristics would remain. We will return to this discussion of the characteristic voids later in this section.

The luminosity spectrum due to Penrose processes for the specific case of quasar 3C 273 is plotted in Figure 1a, along with the observed spectrum for comparison (heavy solid curves superimposed with squares or dots). The outgoing (escaping) luminosity spectrum produced by the Penrose scattered particles is given by (Williams 2002a)

$$\begin{aligned} L_{\nu}^{\text{esc}} &\approx 4\pi d^2 F_{\nu}^{\text{esc}} \text{ (erg/s Hz)} \\ &\approx 4\pi d^2 h\nu^{\text{esc}} f_1 f_2 \cdots f_n (N_{\nu}^{\text{in}} - N_{\nu}^{\text{cap}}), \end{aligned} \quad (1)$$

where d is the cosmological distance of the black hole source; F_{ν}^{esc} is the flux of escaping photons; N_{ν}^{in} and N_{ν}^{cap} are the emittance of incoming and captured photons, respectively; the f_n values define the total fraction of the particles that undergoes scattering [$n = 2$ for PCS and $n = 5$ for PPP ($\gamma\gamma \rightarrow e^-e^+$)]. The values of f_1, \dots, f_n are the fitting factors, which make the Penrose

calculated luminosities agree with observations for the specific case of 3C 273. In short, the f_n values, defined as somewhat free parameters, are probabilities, which are ≤ 1 , but > 0 ; they are dependent on the cross sections—for PCS and PPP, the fraction of the luminosity from the disk intersecting the scattering radii, and the expansion rate of the jet, indirectly related to the the particle densities (Williams 2002a). Note, in the model calculations, if we let every particle scatter, and allow $f_1 = f_3 \sim 10^{-2}$, defining the fraction of the disk luminosity intersecting the scattering regime, with the remaining f_n 's equal 1, the continuum emissions (the top curves on Figures 1a, labeled with numbers for specific cases of target and incident particles) are obtained; see Williams (2002a) for details and complete definitions of the f_n values. The spectrum resulting from the PPP ($\gamma\gamma \rightarrow e^-e^+$) is produced by letting the escaping pairs undergo “secondary Penrose Compton scattering” (SPCS) with low energy (0.03 MeV) radially infalling equatorial accretion disk photons ($\equiv f_3$).

Tables 1 and 2 give model parameters corresponding to some of the numbers on Figure 1a [see Williams (2002a) for other numbers]. On these tables the parameters are defined as follows: r is the scattering radius; E_e is the target electron energy for PCS; $(E_{\mp})_{\text{peak}}$ is the energy value where most of the PPP ($\gamma\gamma \rightarrow e^-e^+$) electrons, used as targets for the SPCS, are created; ν_{ph} is the initial infalling incident photon frequency; ν_{peak} and L_{peak} correspond to the points (solid squares or dots superimposed on the small-dotted or dashed curve, respectively) which give the continuum luminosity resulting from several distributions of PCS or SPCS events (each distribution has 2000 scattering events); L_{obs} is the observed luminosity at ν_{peak} (the average frequency of the interval $\Delta\nu$ where most of PCS or SPCS photons are emitted per 2000 scattering events). Each distribution of 2000 infalling photons have monochromatic energies normalized to the power law distribution for 3C 273 based on observations. The f_n values given in the brackets are values used to fit the general model spectra to agree with specific observations. Overall, to produce the calculated Penrose luminosity spectra of Figure 1a, 74,000 infalling photon scattering events are used.

Thus, as one can see from Figure 1a, the Penrose-Williams mechanism can generate the necessary luminosity observed, and the three model calculated regions of emission [due to PCS by equatorially confined targets (curve passing through nos. 1–7), by nonequatorially confined targets that cross the equatorial plane (curve passing up from 6 through nos. 8–13), and PPP ($\gamma\gamma \rightarrow e^-e^+$) (curve passing through nos. 14–25)] are consistent with the three major regions of emission in all quasars and AGNs. Moreover, taking into consideration the characteristic voids, discussed earlier, proposed to be produced by the different phases of the accretion disk, the lack of participating particles for PCS will cause a void between points 5 and 7 (~ 261 keV – 1.6 MeV) on Figure 1a, indicating a transitional energy regime between a thin disk (~ 3.5 keV) and ion corona (~ 50 keV). Comparing the observed spectrum of 3C 273, it appears that this quasar has a similar accretion disk structure. This suggests that a second void should occur between $7 \text{ MeV} < E < 107 \text{ MeV}$, as it does, agreeing strikingly well with observations between points 16 – 17.

The observed spectra of microquasars (or galactic black holes), in general, appear not to have PCS emission by the nonequatorially confined target electrons, neither the highest energy γ -ray

emission due to PPP ($\gamma\gamma \rightarrow e^-e^+$), suggesting that these sources may not have an ion corona (or ADAF), which would be need to populate the orbits to generate such emission, at least in the highest energy regime (compare Figure 1a). General calculated spectra resulting from a self-consistent thin disk Penrose process model for stellar mass black holes ($\sim 30M_\odot$) appear like a scaled-down Figure 1a (photon luminosity $\sim 10^{38-42}$ erg s $^{-1}$ for total energy range ~ 1 keV–8 MeV), without the curve labeled between points 6–13 (Williams & Hjellming 2002); see § 3.4.4. This is consistent with observations of galactic black holes (Liang 1998).

3.2. The Gravitomagnetic Field and Intrinsically Asymmetrical Polar Jets

The gravitomagnetic (GM) force field is the gravitational analog of a magnetic field. It is the additional gravitational force that a rotating mass produces on a test particle. The GM force is produced by the gradient of $\vec{\beta}_{\text{GM}} = -\omega\hat{\mathbf{e}}_\Theta$, where ω is the frame dragging velocity (Bardeen et al. 1972) and $\vec{\beta}_{\text{GM}}$ is the GM potential (Thorne, Price, & Macdonald 1986). Analysis of the equations governing the trajectories of the Penrose process particles shows that the GM force, which acts proportional to the momentum of a particle, alters the incoming and outgoing momentum parameters of the incident and scattered particles, resulting in asymmetrical polar distributions, and thus, appearing to break the reflection symmetry of the Kerr metric, above and below the equatorial plane (Williams 2002b, 2002a, 1999).¹ Effects of the GM force acting on the PPP ($\gamma\gamma \rightarrow e^-e^+$) process can be discerned from comparing Figures 1d and 1e. When half of the 2000 target photons are allowed to have initial polar coordinate momentum $(P_{\gamma 2})_\Theta > 0$ and the other half $(P_{\gamma 2})_\Theta < 0$, of equal absolute values, with increasing $E_{\gamma 2}$, the e^-e^+ “jet ($+\hat{\mathbf{e}}_\Theta$) to counter-jet ($-\hat{\mathbf{e}}_\Theta$)” ratio ϵ_{\mp} achieves a maximum $\sim 3 : 1$, favoring $(P_{\mp})_\Theta > 0$ (Williams 2002b), as seen in Figure 1e (compare Fig. 1d). The corresponding polar angles of escape for cases of Figures 1d and 1e are displayed in Figures 2a and 2b, respectively. Polar coordinate momentum distributions, $(P'_{\text{ph}})_\Theta$, for escaping PCS photons are displayed in Figure 3, where the primes indicate final conditions. The corresponding polar angles of escape for the cases of Figure 3 are given in Figure 4. Notice the effects of the GM force field causing the (photon jet to counter-jet) ratio ϵ_{ph} to vary from nearly symmetric to asymmetric for the different cases shown. Of these cases the largest ratio achieved is $\sim 5 : 1$ (Figs. 3c and 4c). The direct cause of the asymmetry in the polar direction appears to be due to the severe inertial frame dragging in the ergosphere in which the GM field lines are spacetime dragged in the direction that the black hole is rotating [see Williams (2002b) for details]. The resulting GM force acting on the particles produces the asymmetry.

In most cases, the distribution favors the $+\hat{\mathbf{e}}_\Theta$ direction; however, at particularly low energies, the asymmetry appears to reverse. For example, in the case of PPP ($\gamma\gamma \rightarrow e^-e^+$) at the low initial

¹This effect of symmetry breaking has recently been confirmed by Bini et al. (2003): from a geometrical analysis of GM influence on spiraling Wilkins’ (1972) nonequatorially confined test particle orbits in the Kerr-Taub-NUT spacetime.

energies $E_{\gamma 1} = 3.5$ keV and $E_{\gamma 2} \simeq 3.4$ MeV for the infalling and orbiting photons, respectively, producing escaping e^-e^+ pairs with energies peak around $E_{\mp} \sim 1.5$ MeV, $\epsilon_{\mp} = 700/615 \simeq 1.14$ per 2000 events (Fig. 5a), and after undergoing SPCS (Williams 2002a) per 2000 infalling disk photons ($E_{\text{ph}} = 3.5$ keV), the asymmetry in the final photon polar distribution, for the SPCS, is reverse, with the inverse of the number of particles scattered in the positive polar direction to that in the negative direction $[\epsilon_{\mp(\text{ph})}]^{-1} = 402/165 \simeq 2.44$, favoring the $-\hat{\mathbf{e}}_{\Theta}$ direction (Fig. 5b). This would make the $-\hat{\mathbf{e}}_{\Theta}$ jet appear more energetic and, thus, brighter, since the PPP e^-e^+ polar jets, in this case, are nearly symmetrical, as can be seen in Fig. 5a. Such behavior is consistent with Hjellming and Rupen’s (1995) observations of GRO J1655-40. These authors concluded that the jets themselves must be intrinsically asymmetric, and the sense of the asymmetry must change from event to event. Moreover, they found that the jets lie almost in the plane of the sky, so relativistic beaming cannot explain the observed brightness ratios. [Note, the potential for “jet reversal” due to the GM force field can be seen in eq. (47) of (Williams 2002b): for particle distributions with relatively large $P'_r > 0$ and/or relatively small $P'_\Phi \equiv L'$ —corresponding to small E' .] Also, the jet space velocity Lorentz factor found by these authors ($\Gamma = [1 - (v/c)^2]^{1/2} \approx 2.5 \Rightarrow E \sim 1.3$ MeV) is consistent with the target electron energy, of the SPCS, we have found here, displaying the jet reversal (compare E_{\mp} above and Figs. 5a and 5b), where we are assuming that the bulk velocity of a “blob” is $\sim \langle v_{\mp} \rangle \equiv$ “average” space velocity of the individual PPP electrons per bulk distribution, i.e., assuming $\langle \gamma_{\mp} \rangle \sim \Gamma$, valid at least in the case of the small scale, fast varying galactic black holes; compare Fig. 1f. Thus, the consistency of apparent jet reversal, of these Penrose processes, with observations, gives more compelling evidence that it is probably the Penrose-Williams mechanism at work, close to the event horizon, within r_{ms} , extracting rotational gravitational energy-momentum: in the form of a particle flux, as opposed to the so-called BZ-type models, proposed to extract energy and momentum: in the form of electromagnetic Poynting flux and Alfvén waves, respectively (with the major problem still existing of converting to the necessary particle flux to fuel the observed jets).

Note, a specific possible scenario for the jet reversal in the case of a $30M_{\odot}$ microquasar, similar to that of GRO J1655-40 (Hjellming & Rupen 1995), for a classical thin relativistic accretion disk (Novikov & Thorne 1973), is the following: as secular thermal and density instabilities begin occurring in the inner region of a time dependent accretion disk—commonly referred to as the “Lightman instabilities” (Lightman 1974a, 1974b; Williams 1995, 2002a), kT_e increases to a “reasonable” maximum ~ 30 keV, being consistent with observations. The infalling disk particle electrons with energies $17 \text{ keV} \lesssim E \lesssim 33 \text{ keV}$, and satisfying conditions for a turning point to exist at specific radii (Williams 1995) between $r_{\text{mb}} \lesssim r \lesssim r_{\text{ms}}$, respectively, will be blueshifted according to the gravitational blueshift factor: $32 \gtrsim e^{-\nu} \gtrsim 10.7$, respectively (see § 2), populating the equatorially confined ($Q_e \simeq 0$) target electron orbits with $0.5388 \text{ MeV} \gtrsim E_e \gtrsim 0.3486 \text{ MeV}$, respectively (Bardeen et al. 1972; Williams 1995). This appears to be the catalyst to “turn on” the self-consistent Penrose-Williams mechanism. [Note, the above reasonable maximum energy means before the critical surface density $\Sigma_{\text{crit}}(r)$ is reached (Lightman 1974a, 1974b), which causes the ion coronal/torus two-temperature phase to set in, or before the inner “hot” region

(Novikov & Thorne 1973) extends to $\gtrsim 90M$ (Eardley & Lightman 1975), for $0.001 \leq \alpha \leq 0.1$, $y = 0.6$, and $1 \times 10^{-8} \lesssim \dot{M}/M_{\odot} \text{ yr}^{-1} \lesssim 3 \times 10^{-8}$, where α is the viscosity parameter, y the Kompaneets parameter, and \dot{M} the sub-Eddington accretion rate.] The subsequent escaping PCS X-ray emission becomes more and more asymmetric, favoring the $+\hat{\mathbf{e}}_{\Theta}$ direction, as the infalling initial photon energy is increased, say due to disk instabilities (compare Figs. 3a and 3b). As PCS of infalling disk photons ($E_{\text{ph}} = 3.5 \text{ keV}$) depopulates the equatorially confined target electron orbits, some of the photons with $(P'_{\text{ph}})_r < 0$, $12 \text{ keV} \lesssim E'_{\text{ph}} \lesssim 111 \text{ keV}$, and $Q'_{\text{ph}} \lesssim 0.07M^2m_e^2$, after being blueshifted by $e^{-\nu} \sim 52$, satisfy conditions to have a turning point at the photon orbit (Williams 1995, 2002b), populating, and thus supplying target photons for PPP ($\gamma\gamma \rightarrow e^-e^+$) in the range of $0.6 \text{ MeV} \lesssim E_{\gamma 2} \equiv E''_{\text{ph}} \lesssim 5.8 \text{ MeV}$, respectively, for the range of E'_{ph} above, where $E''_{\text{ph}} = e^{-\nu}E'_{\text{ph}}$. For $E_{\gamma 2} \sim 3.4 \text{ MeV}$, $Q_{\gamma 2} \sim 0.016M^2m_e^2$, as given by the analytical derived expressions of the conserved energy E and angular momentum L of nonequatorially confined particle trajectories (see Williams 1995, 2002b), the subsequent PPP ($\gamma\gamma \rightarrow e^-e^+$) with infalling disk photons $E_{\gamma 1} = E_{\text{ph}}$ (assuming negligible electrons are left in the equatorially confined orbits between r_{ms} , r_{mb}) will produce slightly asymmetrical jets (favoring the $+\hat{\mathbf{e}}_{\Theta}$ direction; compare Fig. 5a). The total energetics due to PCS and PPP ($\gamma\gamma \rightarrow e^-e^+$) at this phase will favor $+\hat{\mathbf{e}}_{\Theta}$, therefore, producing a brighter jet in this polar direction. However, when some of these PPP electrons subsequently interact with infalling disk photons through SPCS, the final emitted escaping photon jets undergo apparent reversal (favoring $-\hat{\mathbf{e}}_{\Theta}$; compare Figs. 5b and 5c): thus, the total energetics will now favor the $-\hat{\mathbf{e}}_{\Theta}$ direction. Compare Figs. 3a, 3b, and 5a–5c, considering the expected time delays (Hjellming & Rupen 1995; Eikenberry et al. 1999a) between the different Penrose processes: PCS, PPP ($\gamma\gamma \rightarrow e^-e^+$), SPCS, and synchrotron emission ($\sim 1.4 - 8.5 \text{ GHz}$) by the escaping PPP electrons (of Fig. 5a): due to, perhaps, their expected intrinsic magnetic field (or an external accretion disk magnetic field), according to $\nu_{\text{syn}} \sim 4 \times 10^6 \gamma_e^2 B$ (Burbidge, Jones, & O'Dell 1974), for $B \sim 10^2 \text{ gauss}$ (Williams 2002a; this assumed value, although consistent with observations, needs further investigation). In addition, some of the PPP electrons (of Fig. 5a) will be created with $E_{\mp} \sim 1.35 \text{ MeV}$, $Q_{\mp} \sim 0.076M^2m_e^2$, $(P_{\mp})_r \sim 7.2m_e$, and $L_{\mp} \sim 5.6Mm_e$ (recall that $G = c = 1$), satisfying the condition to have a turning point at the iso-energy orbit E_{orb} (circular orbit of equal energy at constant radius $r = r_{\text{orb}}$; see Williams 1995), with $E_{\mp} = E_{\text{orb}}$ and $L_{\mp} > L_{\text{orb}}$ at radii $r_{\text{orb}} \sim r_{\text{mb}}$ (the last bound orbit for a material particle, deep within the ergosphere), before escaping to infinity along vortical orbits (§ 3.3), satisfying (Williams 1995)

$$0 < \frac{Q_{\mp}}{E_{\mp}^2} < \frac{Q_{\text{orb}}}{E_{\text{orb}}^2}, \quad (2)$$

or $Q_{\mp} < Q_{\text{orb}}$, implying no turning point in $(P_{\mp})_{\Theta}$, i.e., $(P_{\mp})_{\Theta} \not\rightarrow 0$, yet $(P_{\mp})_r \rightarrow 0$. Some of such electrons can subsequently SPCS infalling disk photons, giving rise to an escaping photon distribution similar to that of Figs. 5b and 5c, favoring $-\hat{\mathbf{e}}_{\Theta}$ (compare Figs. 3 and 5d which favor the $+\hat{\mathbf{e}}_{\Theta}$ direction). Note, this satisfying of the condition to have a turning point at $r_{\text{orb}} \sim r_{\text{mb}}$, before escaping to infinity along vortical trajectories, is also true for the supermassive KBH. Observations of GRO J1655-40 (Hjellming & Rupen 1995) suggest that after the jet outbursts: due to Lightman instabilities, inner region disk depletion, Penrose processes, and plunging orbit (Bardeen et al.

1972) population-depopulation processes, the disk settles back down to its low, “initial” state, to prepare once again to repeat the total *disk instability-Penrose emission cycle*, as described above, indefinitely (i.e., as long as there exists available matter to accrete). Moreover, the disk instabilities are expected to change the accretion rate, thereby causing the Penrose processes to vary.

So, in conclusion of this section, it appears that once the initial requirement has been met: of populating the equatorially confined target electron bound, unstable orbits, inside the ergosphere, between $r_{\text{mb}} \lesssim r \lesssim r_{\text{ms}}$ [at $\sim r_{\text{mb}}$ for maximum PCS energy extraction (Williams 1995)], the KBH operates as a self-consistent system, emitting e^-e^+ and photon jets, relying only on the accretion disk to supply the incident infalling photons, and to populate the initial equatorially confined electron target orbits [i.e., due to disk instabilities (Kafatos & Leiter 1979)]—indicating the beginning of the “cycle.” And within this cycle for particularly low particle initial energies, the GM field can cause the jet brightness asymmetry to reverse. [Note, see Williams (2002b) for a complete description of the relations between the GM field and the space momenta displayed in the figures shown here.] In addition, in the case of quasars-type AGNs (Williams 1995, 2002a), it appears that an ADAF is needed to populate the relatively high energy nonequatorially confined target electron orbits for PCS; and to populate the highest energy photons at the photon orbit for PPP ($\gamma\gamma \rightarrow e^-e^+$), yielding maximum escaping energies $E_{\mp} \sim 54$ GeV (see § 3.1).

3.3. The Vortical Orbits and Intrinsically Collimated Polar Jets

It is found that the Penrose scattered particles escape along vortical trajectories collimated about the polar axis (Williams 1995, 2000, 2002a). These distributions are fluxes of coil-like trajectories of relativistic jet-type particles, escaping out from the equatorial plane at the scattering radius $r < r_{\text{ms}}$, concentric the polar axis. The highest energy particles have the largest P'_Φ values [compare Fig. 1c; compare also Figs. 3b and 4b of Williams (1995)]. Note, P'_r is negative (inward toward the polar axis) for many of the PCS photons (Williams 2002b), and positive for all of the e^-e^+ pairs (compare Fig. 1b). The helical angle of escape $(\delta_i)_{\text{esc}} = |90^\circ - \Theta'|$, of particle type i , relative to the equatorial plane, for the highest energy scattered particles ranges from $(\delta_{\text{ph}})_{\text{esc}} \simeq 1^\circ$ to 30° for PCS (compare Fig. 4) and $(\delta_{\mp})_{\text{esc}} \sim 0.5^\circ$ to 20° for the e^-e^+ pairs (compare Fig. 2); compare also Figs. 6, 7, and 9 of Williams (2002b). The above characteristics of the escaping particles, along with their $|P'_\Theta|$ values (compare Figs. 1d, 1e, 3, and 5), imply strong collimation about the polar axis, giving rise to relativistic jets with particle velocities up to $\sim c$ (compare Fig. 1f). Note, such vortical trajectories and collimation are consistent with the findings of de Felice et al. (de Felice & Curir 1992, de Felice & Carlotto 1997, de Felice & Zanotti 2000), from spacetime geometrical studies of general particle geodesics in a Kerr metric. Moreover, the GM force field, discussed in the last section, responsible for the inertial frame dragging and the asymmetrical jets, also serves to boost the jets into opposite polar directions (Williams 2002b).

3.4. Agreement with Observations

3.4.1. Quasars 3C 273 and 3C 279

In addition to statements made in § 3.1 concerning the model calculated spectra of 3C 273, below I summarize some of the important features resulting from application of the Penrose-Williams mechanism to observations of both 3C 273 and 3C 279; see Williams (2002a) for a thorough description. The observed spectra of both these sources can very well be explained by these Penrose processes and the assumed accretion model, specified in § 2 [see Williams (1995, 2002a) for further details]. As we can see from Figure 1a, there is a striking similarity between the observed spectrum of 3C 273 and the model spectra produced by these Penrose processes. Upon comparing the spectra of radio-loud quasars 3C 273 and 3C 279, based on these Penrose processes, we find the following (Williams 2002a): the shape of the observed spectrum of 3C 273 looks like the “enhanced” (i.e., the highest observed energetic state) spectrum of 3C 279, except for the higher luminosities in 3C 279 and the radio tail in 3C 273. The higher luminosity and the apparent lack of a radio tail in 3C 279 is probably, largely, due to the radiation of 3C 279 being beamed more in the direction of the observer than the radiation of 3C 273. Therefore, the spectrum of 3C 279 has been Doppler blueshifted to an *observed* higher energy interval, and the *apparent* luminosity has been increased. This is consistent with radio observations which detect more superluminal motion (or relativistic beaming near the line of sight of the observer) in 3C 279 than in 3C 273 (Porcas 1987). On the other hand, it seems that 3C 273 has a “hotter” inner accretion disk and is in a predominantly ion torus (or advection dominated) state, as opposed to 3C 279: which appears to oscillates in a highly variable fashion between the thin disk and ion corona phases—for this reason 3C 279 is classified as an optical violent variable (OVV) quasar. The hotter state of the accretion disk (ion torus), which is heated by a runaway thermal instability (Shapiro, Lightman, & Eardley 1976), would result in enhanced Penrose processes [PCS and PPP ($\gamma\gamma \rightarrow e^-e^+$)], and enhanced synchrotron radiation due to the presence of more relativistic electrons, particularly if Eilek’s (Eilek 1980; Eilek & Kafatos 1983) particle reactions ($pp \rightarrow \pi^0 \rightarrow \gamma\gamma \rightarrow e^-e^+$) occur, hence contributing to the prominent observed radio tail of 3C 273. This ion torus/ADAF state appears to be the case always in the continuum emission of 3C 273 and sometimes in the emission spectrum of 3C 279, with 3C 279 not quite achieving the full ion torus status of 3C 273 (Williams 2002a). Thus in summary, the differences in the spectra of 3C 279 and 3C 273 are probably due to (1) the more beaming effect in 3C 279, and (2) the predominantly ion torus/ADAF phase of 3C 273.

3.4.2. Seyfert 1 Galaxy MCG—6-30-15

Recent observations of the bright Seyfert 1 galaxy MCG—6-30-15 [particularly of the broad Fe K α emission line at ~ 6 keV, believed to be originating from the inner accretion disk plasma (Wilms et al. 2001)], and other such type AGNs, are consistent with these model calculations. A qualitative model calculated scenario to explain the observed spectral observations of MCG—6-

30-15, by these Penrose processes, is as follows. Assuming that the plunging orbits of the target electron, inside the ergosphere, have been populated by accretion disk instabilities (as described in § 3.2), self-consistent computer simulations, consistent with MCG—6-30-15, have model parameters for radial infalling photons ($E_{\text{ph}} = 2$ keV) from a thin disk (Novikov & Thorne 1973), that either undergo PCS by equatorially confined orbiting target electrons ($E_e \simeq 0.539$ MeV) at r_{mb} , or PPP ($\gamma\gamma \rightarrow e^-e^+$) at r_{ph} . The blueshifted energies (due to frame dragging) attained by the $\sim 31\%$ up to 83% escaping particles, returning to the disk to be reprocessed and/or escaping to infinity, are the following: for PCS photons, $E'_{\text{ph}} \sim 5.2 - 175$ keV for equatorially confined orbiting target electrons, with relative incoming and outgoing photon luminosities $(L_{\gamma})_{\text{out}} \sim 0.014 - 11 (L_{\gamma})_{\text{in}}$, respectively, where $(L_{\gamma})_{\text{in}} \sim 2.5 \times 10^{45}$ erg s $^{-1}$; and for the relativistic PPP electrons (with $E_{\gamma 1} \equiv E_{\text{ph}}$ and $E_{\gamma 2} \simeq 4.8$ MeV), $E_{\mp} \sim 2.4$ MeV [consistent with synchrotron radiation into the radio regime for $B \sim 10^2$ gauss, and inverse Compton scattering (SPCS of disk photons) into the X-ray/soft γ -ray regime—with relative incoming and outgoing photon luminosities $(L_{\gamma})_{\text{out}} \sim 0.006 - 2.7 (L_{\gamma})_{\text{in}}$, for $M \sim 10^8 M_{\odot}$, at ~ 71 keV – 1.3 MeV, respectively], suggesting relatively weak, less powerful and less prominent radio jets, i.e., a radio quiet AGN, like a Seyfert galaxy (compare Figs. 1a, 5a and 5b for similarities and dissimilarities). Note, for self-consistency, $E_{\gamma 2}$ is assumed based on prior PCS photons with $(P'_{\text{ph}})_r < 0$ that satisfy conditions for the existence of a turning point at the photon orbit (Williams 2002b). Note also that, at these low energies for $E_{\gamma 1}$ and $E_{\gamma 2}$, the SPCS polar jets appear to “flip,” undergoing brightness jet reversal (as discussed in § 3.2), differing by a factor ~ 10.6 , in particle numbers, favoring $-\hat{\mathbf{e}}_{\Theta}$ (compare Fig. 3 and Figs. 5b – 5d), whereas the initial PPP target electron polar jets, differ by a factor ~ 2 favoring $+\hat{\mathbf{e}}_{\Theta}$ (compare Fig. 5a). The PCS photon distribution in the range of E'_{ph} above, emitted from $r_{\text{mb}} < r_{\text{ms}}$, with the highest energy photons concentrated in the equatorial plane, is expected to be consistent with the observed extremely steep emissivity profile $\beta \sim 4.3 - 5.0$ of Wilms et al. (2001), indicating that most of the Fe K α line emission originates from the inner region of a relativistic accretion disk; compare Figure 4. Specific details of the emissivity $\varepsilon(r) \propto r^{-\beta}$ of these Penrose processes, particularly of the PCS, will be presented in a future paper by the author.

3.4.3. Radio Galaxy M87

Recent radio observations of active galaxy M87 (Junor et al. 1999) suggest that electromagnetic collimation becomes important at radii $\gtrsim 30 - 100 r_g$, wherein the initial “open angle” of the jet $\sim 60^\circ$ (at radii $< 30 r_g$) is made smaller to $\sim 30^\circ$ by the electromagnetic field, where $r_g = 2M$ ($= r_0$, the radius of the ergosphere at the equator). This is consistent with the Penrose mechanism providing (in addition to the relativistic particles) the initial collimation at radii ($< 30 r_g$), i.e., closer to the black hole. Since M87 is a giant elliptical galaxy, this could mean that its geometric configuration is possibly helping to maintain the initial collimation by the black hole: which begins at $r < r_g$, and must extend out to at least $\sim 30 r_g$ —i.e., until, it appears, electromagnetic collimation takes over. However, before one can say for certain of the electromagnetic processes occurring, a time dependent MHD evolution of the Penrose escaping particle plasma must be performed (presently

under investigation by the author). That is, it should not be ruled out that the intrinsic collimation due to the black hole, of the escaping relativistic plasma: and any associated “dynamo” generated magnetic field, may be sufficient to maintain collimation.

Further, concerning M87, its observed spectrum in general can be explained by the Penrose mechanism presented in this paper. Some observational properties of M87 are the following (Eilek 1997): $L_{\text{jet}} \sim 10^{43-44} \text{ erg s}^{-1}$; striking comparisons of radio (Very Large Array) and optical (Hubble Space Telescope) images of the jet; optical and possibly X-ray emission believed to be of synchrotron origin; and more recently, the mid-IR observations (Perlman et al. 2001) showing that the nuclear IR emission is entirely consistent with synchrotron radiation, and there is no evidence for thermal emission from a dusty nuclear torus. Based on these properties the following scenario can be devised according to the Penrose-Williams mechanism. The jet is no doubt beamed, since observed superluminal motions give apparent velocities up to $\sim 6c$, implying line-of-sight angle $\theta_s \sim 10^\circ - 19^\circ$, bulk Lorentz factor $\Gamma \sim 6 - 40$, jet Doppler factor $\delta_* \sim 5.7 - 0.5$, and jet brightness boost $\delta_*^3 \sim 190 - 0.1$, respectively (Biretta, Sparks, & Macchetto 1999; see also Williams 2002a). M87 is probably an evolved blazar-type AGN (OVV quasar and BL Lac object). Its luminosity spectrum (although less powerful, less energetic) most likely resembles that of 3C 279 (§ 3.4.1; see also Williams 2002a). The most noticeable change in the spectrum from times past is probably the lack of high energy γ -rays: due to the lack of the availability of infalling low energy (soft X-ray) disk photons, or the lack of high energy PPP ($\gamma\gamma \rightarrow e^- e^+$) electrons, to undergo effective SPCS—i.e., resulting in escaping trajectories for the scattered γ -rays. Since the jet of M87 is still seen prominently in the radio/optical/X-ray, an optically thin hot ion torus, PCS, PPP ($\gamma\gamma \rightarrow e^- e^+$), and subsequently synchrotron radiation of the PPP electrons (particularly into the optical: implying $E_{\mp} \sim 177 - 558 \text{ MeV}$ for $B \sim 10^{3-2} \text{ gauss}$, respectively), are consistent with the observations. The parenthetical statement above suggests that the magnetic field producing the synchrotron radiation may be that of the escaping Penrose plasma rather than that of the popular proposed large scale dipolar-like field of the accretion disk (since large scale, strength dipolar accretion disk fields are in practice difficult to create); this however requires an investigation. Moreover, besides coming from the inner region of a relativistic thin disk (Novikov & Thorne 1973), there are three possibilities for producing the observed soft X-ray emission, within the confinements of the Penrose-Williams mechanism: (1) a synchrotron origin requires electron energies $\sim 17 \text{ GeV}$ ($\gamma_e \sim 3 \times 10^4$) for $\sim 2 \text{ keV}$ emission at $B \sim 10^2 \text{ gauss}$, and could very well be produced by the PPP ($\gamma\gamma \rightarrow e^- e^+$), at least for ultrarelativistic $e^- e^+$ pairs up to $\sim 54 \text{ GeV}$ for B as low as $\sim 10 \text{ gauss}$; (2) the nonthermal X-rays are due to a low absolute efficiency PCS (Williams 1995), at least for X-rays emanating from the core (compare § 3.1, item 3.a); and (3) the jet is beamed, and self-Compton scattering of lower energy radio and IR synchrotron photons by the escaping, intrinsically polar collimated PPP electrons is occurring: the observed energies of the inverse/self-Compton scattered photons are blueshifted due to Doppler boosting into the optical and X-ray regimes, respectively, according to $E_{\text{Comp}} \simeq 0.5\gamma_e^2 h\nu$ (Dermer, Schlickeiser, & Mastichiadis 1992) for $\Gamma = 6$, $\theta_s = 10^\circ$. Now, all three items above could occur concurrently, more or less; however, since superluminal motion appears to be important in M87, item (3) is most likely the dominant, yet, not to rule out the

other items. If this dominance is true, then the energies of the jet electrons need only be as high as $E_{\mp} \sim 20 - 150$ MeV for $B \sim 10^2$ gauss. This is consistent with the Penrose processes described here, in the presence of a thin disk/ion corona accretion—without the need of Eilek’s π^0 decays to populate the photon orbit (see § 3.1, items 2.a – 2.c). Note, such ion coronas or tori are poor radiators, and expected to be of relatively low density, with 30 keV $\lesssim kT_e \lesssim 50$ keV; this may account for the lack of evidence for an inner “dusty” torus emitting thermal radiation in the mid-IR observations by Perlman et al. (2001). However, it still seems unlikely that such a low electron energy and particle density ion torus (or ADAF) can be jet fuel for the BZ-type models near the event horizon, inside the ergosphere, as required by such models (Blandford & Begelman 1999). [See Williams (2002a) for a complete description of the accretion disk model consistent with these Penrose processes and observations.] Nevertheless, such BZ-type models (e.g., Punsly 1991; Koide et al. 2000) appear to be important at $r > 30r_g$, as suggested by observations (Junor et al. 1999), particularly if the Penrose-Williams particles are used as fuel.

3.4.4. Galactic Black Hole X-Ray Source Cygnus X-1

The Penrose-Williams model presented here applies to all mass size KBHs, with the stellar mass black hole appearing as a scaled-down supermassive. When the parameters are expressed in gravitational units ($c = G = 1$), the Penrose process emission energy-momentum spectra (P_r vs. E ; P_{Θ} vs. E ; P_{Φ} vs. E) over the range of masses are approximately identical. The luminosity spectra of these Penrose processes for the different masses, in general, span over a range $\sim 10^{39} - 10^{52}$ erg s $^{-1}$ (compare Figs. 1a and 6). In general, the differences of the Penrose process output luminosities between supermassive KBHs and “micro-massive” KBHs are determined by the bolometric luminosity of the incoming photons (Eilek 1980; Williams 2002a), directly dependent on the accretion rate, which is governed by the surrounding accretion disk environment. For example, the observations of the classical stellar/galactic black-hole candidate Cygnus X-1 (Liang 1998) can be explained by these Penrose processes: Processes consistent with Cyg X-1 have model parameters for radial infalling photons ($E_{\text{ph}} = 3.5$ keV) from a thin disk (Novikov & Thorne 1973), that either undergo PCS by equatorially confined orbiting target electrons ($E_e \simeq 0.539$ MeV) at r_{mb} or PPP ($\gamma\gamma \rightarrow e^-e^+$) at r_{ph} . The blueshifted energies (due to frame dragging) attained by the $\sim 82\%$ up to 92% escaping particles, returning to the disk to be reprocessed and/or escaping to infinity, are the following: for the PCS photons, $E'_{\text{ph}} \sim 12 - 250$ keV, with relative incoming and outgoing photon luminosities $(L_{\gamma})_{\text{out}} \sim 0.4 - 130 (L_{\gamma})_{\text{in}}$, respectively, where $(L_{\gamma})_{\text{in}} \sim 4 \times 10^{38}$ erg s $^{-1}$; and for the relativistic PPP electrons (with $E_{\gamma 1} \equiv E_{\text{ph}}$ and $E_{\gamma 2} \sim 5$ MeV), $E_{\mp} \sim 4$ MeV [consistent with synchrotron radiation into the radio regime for $B \sim 10^2$ gauss, and inverse Compton scattering (SPCS of disk photons) into the hard X-rays/soft γ -ray regime—with relative incoming and outgoing photon luminosities $(L_{\gamma})_{\text{out}} \sim 8 - 2000 (L_{\gamma})_{\text{in}}$, for $M \sim 30M_{\odot}$, between ~ 100 keV–3 MeV]; compare Figure 6; see Williams & Hjellming (2002) for further details. Note, for self-consistency, $E_{\gamma 2}$ is assumed based on prior PCS photons with $(P'_{\text{ph}})_r < 0$ that satisfy conditions for the existence of a turning point at the photon orbit (Williams 2002b). Note also that, as in the cases of GRO

J1655-40 (§ 3.2) and MCG—6-30-15 (§ 3.4.2), at these low energies for $E_{\gamma 1}$ and $E_{\gamma 2}$, the SPCS polar jets undergo slight so-called jet reversal (as discussed in § 3.2), differing by a factor ~ 1.4 favoring $-\hat{\mathbf{e}}_{\Theta}$, whereas the initial PPP target electron polar jets, differ by a factor ~ 1.1 favoring $+\hat{\mathbf{e}}_{\Theta}$ (compare Figs. 3a, 3b, and 5).

In the above model for Cyg X-1, the PPP electron energy E_{\mp} can increase to $\gtrsim 10$ MeV, as the infalling thin disk photon energy for PCS by equatorially confined target electrons is increased to $\sim 20 - 30$ keV (Williams & Hjellming 2002), say due to disk instabilities (compare § 3.2). This appears to be the case for Cyg X-1 when in its “high” state (McConnell et al. 1989), and to explain the persistent power-law γ -ray tail up to ~ 20 MeV (McConnell et al. 1994).

Moreover, concerning \sim kHz quasi-periodic oscillations (QPOs) observed in galactic black holes (Strohmayer 2001; Remillard et al. 2002; Abramowicz et al. 2002), such QPOs can be predicted from the Penrose scattering processes described here. The “QPOs” of, say, a given local distribution of neighboring target electrons, responsible for PCS into the X-ray/soft γ -ray regime, emitting from geodesic orbits at radii between r_{ms} and r_{mb} , can be obtained from (Bardeen et al. 1972)

$$\Omega = \frac{e^{\nu} v_{\Phi}}{\sqrt{g_{\Phi\Phi}}} + \omega, \quad (3)$$

where $\Omega \equiv d\Phi/dt$ is the coordinate angular velocity of a circular orbit; e^{ν} is the inverse of the blueshift factor (see § 2), commonly referred to as the “redshift” factor; v_{Φ} is the orbital velocity in the azimuthal direction of the target particles relative to the LNRF, i.e., as measured by a general observer at rest relative to this frame (Bardeen et al. 1972; see also Williams 1995); $e^{\psi} = \sqrt{g_{\Phi\Phi}}$ is the radius of the circumference about the axis of symmetry (Thorne et al. 1986). So, with the frame dragging *angular* velocity given by $\omega = \omega(r, a = 0.998M, M = 30M_{\odot}, \Theta = \pi/2)$, we find the predicted range to be between: $\nu_{\text{QPO}} = (\Omega_{\text{QPO}}/2\pi) \simeq 467$ Hz, $\simeq 506$ Hz at r_{ms} , r_{mb} , respectively, corresponding to periods ~ 2 ms, as measured by an observer at infinity. Note, the counterpart QPOs for a supermassive ($10^8 M_{\odot}$) KBH are $\sim 2 \times 10^{-4}$ Hz; this relatively low frequency is probably the reason these counterpart QPOs have yet to be detected in sources harboring such massive KBHs (see Miller et al. 2002 and references therein). These calculations suggest that \sim kHz QPOs may also be due to the inertial frame dragging of the nonequatorially confined target particles’ orbital “ring” at scattering radius r (Williams 1995), particular of the nodes (points at which the orbit, in going between negative and positive latitudes, intersects the equatorial plane)—which happens to be where the most effective Penrose scattering processes would occur, as resulting emitting regions of neighboring particles sweep across the line of sight of the observer. In this case, the observed oscillation frequencies might be slightly smaller (between $\nu_{\text{QPO}} \simeq 439$ Hz, $\simeq 494$ Hz at r_{ms} , r_{mb} , respectively) and appear twice as fast as those given above or in pairs.² See Williams (2002b) for a discussion of the nonequatorially confined spherical-like orbits, first proposed by Wilkins (1972). The above findings are consistent with the QPOs proposed to originate from orbits within the

²Similar effects have been independently suggested by Stella, Vietri, and Morsink (1999), concerning nodal precession, and by Cui, Zhang, and Chen (1998) as evidence of frame dragging around spinning black holes.

radius of the marginal stable orbit r_{ms} (Zhang, Shrohmayer, & Swank 1997) and the suggestion that the energy distribution of the energetic electrons must be oscillating at the QPO frequency (Morgan, Remillard, & Greiner 1997).

Note, in the above qualitative, yet self-consistent models, for the radio quiet Seyfert galaxy ($\sim 10^8 M_\odot$; § 3.4.2) and the galactic black hole Cyg X-1 ($\sim 30 M_\odot$), for the initial conditions used based on properties of the accretion disk, the main differences in the emitted spectra are the number of Penrose produced e^-e^+ pairs escaping, and the range of E_\mp : for the Seyfert galaxy E_\mp is in the narrow range $\sim 2.2 - 2.6$ MeV, and for the galactic black hole, $E_\mp \sim 0.8 - 4$ MeV. In both cases, most (if not all) of the PPP electrons have turning points in the nonequatorially confined (spherical-like) electron orbits at $\sim r_{\text{mb}}$, as discussed in § 3.2, indicating that these electrons escape along vortical trajectories collimated about the polar axis, without interacting appreciably with the inner edge of the bound stable accretion disk (located at $\sim r_{\text{ms}}$): this is also true in the high energy regime for the supermassive KBH (see Williams 2003).

4. Conclusions

From the Penrose-Williams model presented here to extract energy-momentum from a rotating black hole we can conclude the following: PCS is an effective way to boost soft X-rays to hard X-rays and γ -rays up to $\sim 7 - 14$ MeV. PPP ($\gamma\gamma \rightarrow e^-e^+$) is an effective way to produce relativistic e^-e^+ pairs up to $\sim 10 - 54$ GeV: This is the probable mechanism producing the fluxes of relativistic pairs emerging from cores of AGNs; and when relativistic beaming is included, apparent energies \sim TeV can be achieved (Williams 2002a). These Penrose processes can operate for any size rotating black hole, from quasars to microquasars (i.e., galactic black holes). Overall, the main features of quasars: (a) high energy particles (X-rays, e^-e^+ pairs, γ -rays) coming from the central source; (b) large luminosities; (c) collimated jets; (d) one-sided (or uneven) polar jets—which under certain conditions the asymmetry brightness appears to “flip,” can all be explained by these Penrose processes.

Moreover, it is shown here that the geodesic treatment of individual particle processes close to the event horizon, as governed by the black hole, is sufficient to described the motion of the particles. This is consistent with MHD that the behavior of such individual particles on geometry (or gravity)-induced trajectories is also that of the bulk of fluid elements in the guiding center approximation (de Felice & Zanotti 2000). In light of this, MHD should be incorporated into these calculations, particularly to describe the flow of the Penrose escaping particles away from the black hole, i.e., to perhaps further collimate and accelerate these jet particles out to the observed distances.

Importantly, it is also concluded, that, the difference between quasars and radio quiet, radio loud galaxies, and microquasars, appears to be the presence or the lack of a two-temperature ADAF: with or without nuclear reactions (undergoing particle reactions $pp \rightarrow \pi^0 \rightarrow \gamma\gamma \rightarrow e^-e^+$)

in the inner region of the accretion disk (see Eilek 1980; Eilek & Kafatos 1983). In the case of the radio quiet, radio loud galaxies the ADAF may no longer be “nuclear reactive,” however just hot, and in some cases the disk may have evolved back to its thin disk phase, including the associated Lightman instabilities (Lightman 1974a, 1974b). The microquasars, on the other hand, appear in general not to satisfy the condition for the existence of an ADAF, which is determined by the accretion rate (Williams & Hjellming 2002).

Finally, what makes the Penrose mechanism described here so admirable is that it allows one to relate the macroscopic conditions, i.e., of the global gravitational field of the KBH, to the microscopic world of particle physics. This description, which is being proven by observations, to be the correct description, allows us to see directly how energy is extracted from a black hole. The physics used in this Penrose analysis is that of special and general relativity. From this analysis and its consistency with observations, we arrive at the following conclusion: Close to the event horizon, gravity and particle-particle interactions, in the ergosphere, of highly curved spacetime (where the effect of the external accretion disk magnetic field is apparently negligible), are sufficient to described energy-momentum extraction from a rotating black hole.

I first thank God for His thoughts and for making this research possible. Next, I thank Dr. Fernando de Felice and Dr. Henry Kandrup for their helpful comments and discussions. Also, I thank Dr. Roger Penrose for his continual encouragement. I am grateful to the late Dr. Robert (Bob) Hjellming for his helpful discussions and cherished collaboration. Finally, I thank the anonymous referee for helpful comments. Part of this work was done at the Aspen Center for Physics. This work was supported in part by a grant from NSF at NRAO and AAS Small Research Grant.

APPENDIX

Associated problems with popular MHD models are described below:

1. In order to explain observations of the Seyfert 1 galaxy MCG—6-30-15, that copious photons are been extracted from the black hole from radii less than the marginal stable orbit r_{ms} ($\simeq 1.2M$, in gravitational units with $G = c = 1$, where M is the mass of the black hole), it has been claimed that the force lines of the disk magnetic field \mathbf{B}_d couple with matter deep within the “plunging” region $< r_{\text{ms}}$, thereby extracting rotational energy in the form of electromagnetic energy (Wilms et al. 2001; Krolik 2000). However, the first detailed numerical relativistic time-dependent MHD calculations in a Kerr metric (Koide et al. 2000; Meier & Koide 2000; Meier, Koide, & Uchida 2001) show that in order for magnetic field lines to extend inward to the numerical limited radius $1.3M$ —being frozen to the plasma, of Keplerian velocity, the disk material must be initially counter rotating: opposite the direction that the black hole is rotating. This appears inconsistent with the observations of Zhang, Cui, & Chen (1997) and in general the physics occurring inside the ergosphere in which inertial frames are dragged in the direction that the black hole is rotating.

Even though we know that particles can have retrograde orbits inside the ergosphere, relative to an observer at infinity, it is highly improbable that the whole disk of matter will be counter rotating, at least in the general sense. Further, it appears that the net rotational energy being “extracted” in the numerical simulation of these authors (Koide et al. 2000) in the form of electromagnetic energy over and above the gravitational binding energy released due to the hydrodynamic energy transported into the black hole is merely the rotational energy from the nonphysical initial condition that the accretion disk plasma is counter rotating as it falls into the ergosphere.³ On the other hand, for a co-rotating disk these authors found that the inward limiting radius is even larger ($\sim 6M$), attributed to a centrifugal barrier (Koide et al. 2000). Although this time-dependent MHD model is an excellent representation of subrelativistic ($\lesssim 0.4c$) jet formation in a KBH magnetosphere, the inconsistencies of this MHD model, as matter nears the event horizon ($r_+ \simeq 1.063M$), is probably an indication of the limitation, of such fluid dynamical models, in describing energy extraction from a rotating black hole: this being based on the guiding center approximation, wherein the single-particle approach is essential close to the black hole (de Felice & Carlotto 1997; de Felice & Zonotti 2000), i.e., the behavior of individual particles is also that of the bulk of fluid elements. This means that gravitational-particle interactions, such as the Penrose processes described here (in this paper), are required. Note, in these Penrose processes, which occur close to the event horizon, electromagnetic and atomic forces dominate on the microscopic scale, while gravity is dominant on the macroscopic scale—thus, as it should be in the strong gravitational potential well of the KBH; but far away from r_+ electromagnetism appears to dominate macroscopically (Junor, Biretta, & Livio 1999). Moreover, stability of the co-rotating disk, falling inward to the limiting radius $\sim 6M$, at the Keplerian velocity, when magnetic field lines are coupled to the infalling plasma, with the jet formation similar to that of the Schwarzschild black hole case (Koide, Shibata, & Kudoh 1999), suggests that the large scale magnetic field plays a dominant role at large distances from r_+ , irrespective of whether or not the black hole is rotating. In addition, these numerical inward limiting radii, at least in the case of the counter-rotating disk ($\sim r_{\text{ms}}$), may also be a display of the horizon being a “vacuum infinity” (Punsly & Coroniti 1989; Punsly 1991; Williams 2002a): to the charge neutral disk particle plasma, and its associated magnetic field, in accordance with the “no-hair” theorem (Carter 1973; Misner, Thorne, & Wheeler 1973; Williams 1995), suggesting that the interaction of the disk magnetic field with particles in bound, trapped orbits at $r < r_{\text{ms}}$ is negligible compared to the Penrose gravitational-particle interactions described here. Therefore, it appears that electromagnetic energy cannot be effectively extracted from the so-called plunging region: where gravitational-particle interactions will clearly dominate if the flux of $\mathbf{B}_d \rightarrow 0$, as it does in general nearing the vacuum infinity horizon [Punsly & Coroniti 1989; Punsly 1991; Williams 2002a; see also Bičák (2000) and Bičák & Ledvinka (2000) for a detailed general relativistic

³Moreover, these authors (Koide et al. 2000) made the statement that inside the “static limit” (i.e., ergosphere), the velocity of the frame dragging exceeds the speed of light ($c\Omega_3/\alpha > c$)! Not only is this an untrue statement, but it is a violation of the laws of physics. The frame dragging circular velocity inside the ergosphere as measured by an observer at infinity is $\omega\sqrt{g_{\Phi\Phi}} \sim 0.8 - 0.9c$ (see Bardeen et al. 1972; Misner et al. 1973; Thorne et al. 1986; Williams 1995; see also § 3.4.4).

calculation showing this]. Note, the encountered centrifugal barrier for the co-rotating disk, which supports the role of the magnetic field acting prevalently at sufficiently large distances from the central black hole source, can probably be overcome somewhat if an effective transfer of angular momentum outward exists, such as that due to viscosity, magneto-rotational instability (Balbus & Hawley 1991), and, possibly, the gravitomagnetic field (Williams 2002b). Moreover, the highly-idealized MHD model of Koide et al. (2002) does not resolve the issues discussed above. Finally, in the BZ-type models, the assumption that electromagnetic energy flux (or Poynting flux) is flowing out of the event horizon, in the observer’s frame at infinity (Blandford 2000), is a violation of the no-hair theorem.

2. To convert the electromagnetic energy to particle energy at the event horizon, and to duplicate the observed luminosities from a Poynting flux, it requires a large-scale magnetic field strength $B_d \sim 10^4(M/10^7M_\odot)^{-1}$ gauss (Wilms et al. 2001; Blandford & Znajek 1977). In order to create e^-e^+ pairs along the field lines, as in the case of pulsars, a field strength of at least $B_d \sim 10^{12}$ gauss is needed (Sturrock 1971; Sturrock, Petrosian, & Turk 1975). (The mechanism, however, for the generation of the pairs in an electromagnetic field to date is a subject of debate.) The first of the large strengths required above appears to be achieved for supermassive KBHs, at present—i.e., with speculated assumptions. But for galactic black holes (microquasars) with masses $\sim 10M_\odot$, $B_d \sim 10^{10}$ gauss seems highly impossible to generate from, in most cases, a binary system accretion disk plasma flow. An effective model for AGNs must also operate for microquasars as well. Moreover, according to electrodynamics, in general, to lift the particles “frozen” to the magnetic field lines, from a disk, accelerating them to relativistic speeds, there has to be an electric field component E_z (Lovelace 1976). However, there exist problems in generating sufficient \mathbf{E} parallel to the polar direction ($\pm \hat{\mathbf{e}}_z$ axis); none of the polar MHD models of this particular type adequately gets rid of this problem. Magnetic reconnection may be a solution to some degree.

3. To get around problems in items 1 and 2 (specifically, the large strength field required and the vacuum infinity horizon) it is assumed that a “hot” ion corona or torus-like accretion can provide the necessary jet particles: (a) for the magnetosphere to act on, accelerating and collimating through centrifugal driving winds (see below); and (b) to provide the hot ram pressure, to “ram” the magnetic field lines inward to the event horizon. However, now there appears to be a problem as far as how to liberate particles from trapped orbits inside the ergosphere (particularly in the plunging regions) onto escaping orbits. Particles in plunging regions, as defined by Bardeen, Press, and Teukolsky (1972), i.e., particles originating from infinity, with $E/\mu_o \geq 1$, can only escape, by being injected onto escaping orbits by some physically process near the black hole—such as the Penrose scattering processes described here—since nothing can come out of the hole (Bardeen et al. 1972). Therefore, again, the BZ-type models are faced with the same old challenge, and an even greater one, as the magnetic field is assumed to get closer to the KBH: where general relativistic effects must be considered, i.e., how do we get the necessary escaping particles in numbers out of the ergospheric region ($< r_{ms}$) into the jets, and then out to the observed distances? Now, with observations showing M87 not having the expected large “dusty” thermal IR-emitting torus

(Perlman et al. 2001) that could have possibly served as particle jet “fuel” for a BZ-type model, the Penrose mechanism to extract energy-momentum, as described by Williams (1995), the so-called Penrose-Williams mechanism, appears to be the only possible, plausible way to power this AGN, and thus, generate its jets (§ 3.4.3). So, in summary, associated with the BZ-type MHD models, there exists the historical problem that I ran into years ago with such models in 1988: How does one convert from electromagnetic energy to the particle energies observed in the jets, emanating from the region where energy is observed to be extracted, i.e., inside the ergosphere close to the event horizon? None of the existing BZ-type MHD models thus far adequately solves this “age-old” problem.

4. In the centrifugal driven winds (Blandford & Payne 1982) mentioned above, the following is assumed: If the disk magnetic field lines subtends an angle of more than $\pm 30^\circ$ to the rotation axis, the gas will be flung away from the disk into collimated jets with speeds a few times the escape velocity at the magnetic footprint on the disk. This may be true at $r \gg r_+$, but near the event horizon r_+ , the escape conditions (see Williams 1995) must be adequately applied. Such general relativistic treatment of the Blandford & Payne (1982) model calculations has yet to be done in any MHD model relying on centrifugal driven winds to power the jets.

5. To clear up any confusion, the authors of the historical paper (Wilms et al. 2001) loosely called the BZ-type models the Penrose effect—the very name for years that had distinguished Williams’ (1991, 1995, 1999, 2001) internationally known successful 4-D Penrose model (see also Piran & Shaham 1977; Leiter & Kafatos 1978; Kafatos & Leiter 1979; Kafatos 1980; Wagh & Dadhich 1989) from the BZ-type models. Strangely, these authors did not reference Williams’ investigation. Nevertheless, to set the record straight, the Penrose mechanism [as summarized here and described in details in Williams (1995)], which involves gravitational extraction of energy from a spinning black hole, as primarily visualized by Penrose (1969), and that of the so-called BZ mechanism, which involves electromagnetic extraction of energy (Blandford & Znajek 1977), are two very different models. So different that the statement made by the authors in Wilms et al. (2001), “For parameters relevant to our discussion, the extra energy source is provided by the spin via the Penrose effect occurring within the radius of marginal stability (but outside of the stretched horizon),” indeed requires a proper reference, since Williams’ model is popularly known as the only existing completely worked out model of the Penrose mechanism: occurring within the radius of marginal stability r_{ms} . Whatever the case may be, the recent observations of MCG—60-30-15 (Wilms et al. 2001) and M87 (Perlman et al. 2001) introduce compelling evidence confirming that perhaps it is the effects of Williams’ black hole source model being observed (as described in this paper), and hardly those of the BZ-type models. The evidence presented here strongly suggests that observed black hole sources have a central energy generation similar the mechanism described in this paper. So, to avoid any further confusion, it seems appropriate to refer to Williams’ model as the Penrose-Williams mechanism, which I interchangeably refer to as just the Penrose mechanism, out of respect for its originator Penrose (1969).

REFERENCES

Abramowicz, M. A., Bulik, T., Bursa, M., & Kluzniak, W. 2002 (astro-ph/0206490)

Balbus, S. A., & Hawley, J. F. 1991, ApJ, 376, 214

Bardeen, J. M. 1973, in Black Holes, ed. C. DeWitt & B. S. DeWitt (New York: Gordon and Breach Science Publishers), 215

Bardeen, J. M., Press, W. H., & Teukolsky, S. A. 1972, ApJ, 178, 347

Bičák, J. 2000, Pramana, 55, No. 4, 481 (gr-qc/0101091)

Bičák, J. & Ledvinka, T. 2000, Nuovo Cimento, 115 B, 739 (gr-qc/0012006)

Bini, D., Cherubin, C., Jantzen, R. T., & Mashhoon, B. 2003, Class. Quantum Grav., 2, 457 (gr-qc/0301055)

Biretta, J. A., Sparks, W. B., & Macchetto, F. 1999, ApJ, 520, 621

Blandford, R. D. 2000, in Proc Discussion Meeting on Magnetic Activity in Stars, Discs and Quasars. Ed. D. Lynden-Bell, E. R. Priest and N. O. Weiss. To appear in Phil. Trans. Roy. Soc. A (astro-ph/0001499)

Blandford, R. D., & Begelman, M. C. 1999, MNRAS, 303, L1

Blandford, R. D., & Payne, D. G. 1982, MNRAS, 199, 883

Blandford, R. D., & Znajek, R. L. 1977, MNRAS, 179, 433

Boyer, R. H., & Lindquist, R. W. 1967, J. Math. Phys., 8, 265

Burbidge, G. R., Jones, T. W., & O'Dell, S. L. 1974, ApJ, 193, 43

Carter, B. 1968, Phys. Rev., 174, 1559

Carter, B. 1973, in Black Holes, ed. C. DeWitt, & B. S. DeWitt (New York: Gordon and Breach Science Publishers), 57

Cui, W., Zhang, S. N., & Chen, W. 1998, ApJ, 492, L53

de Felice, F., & Calvani, M. 1972, Nuovo Cimento, 10B, 447

de Felice, F., & Carlotto, L. 1997, ApJ, 481, 116

de Felice, F., & Curir, A. 1992, Class. Quantum Grav., 9, 1303

de Felice, F., & Zanotti, O. 2000, Gen. Rel. Grav., 8, No. 32, 1449 (astro-ph/9912413)

Dermer, C. D., Schlickeiser, R., & Mastichiadis, A. 1992, A&A, 256, L27

Eardley, D. M., & Lightman, A. P. 1975, *ApJ*, 200, 187

Eikenberry, S. S., Matthews, K., Morgan, E. H., Remillard, R. A., & Nelson, R. W. 1999a, *ApJ*, 494, L61 (astro-ph/9710374)

Eikenberry, S. S., Matthews, K., Murphy, T. W., Morgan, E. H., Remillard, R. A., & Muno, M. 1999a, *ApJ*, 506, L31 (astro-ph/9807204)

Eilek, J. A. 1980, *ApJ*, 236, 664

Eilek, J. A., & Kafatos, M. 1983, *ApJ*, 271, 804

Heinz, S., Choi, Y.-Y., Reynolds, C. S., & Begelman, C. 2002, *ApJ*, in press (astro-ph/0201107)

Hjellming, R. M., & Rupen, M. P. 1995, *Nature*, 375, 464

Junor, W., Biretta, J. A., & Livio, M. 1999, *Nature*, 401, 891

Kafatos, M. 1980, *ApJ*, 236, 99

Kafatos, M., & Leiter, D. 1979, *ApJ*, 229, 46

Kerr, R. P. 1963, *Phys. Rev. Lett.*, 11, 237

Koide, S., Meier, D. L., Shibata, K., & Kudoh, T. 2000, *ApJ*, 536, 668

Koide, S., Shibata, K., & Kudo, T. 1999 *ApJ*, 522, 727

Koide, S., Shibata, K., Kudo, T., & Meier, D. L. 2002, *Science*, 295

Krolik, J. H. 1999, *ApJ*, 515, L73

Krolik, J. H. 2000, in *Explosive Phenomena in Astrophysical Compact Objects, Proceedings of the 1st KIAS Astrophysics Workshop* (astro-ph/0008372)

Leiter, D. & Kafatos, M. 1978, *ApJ*, 226, 32

Liang, E. P. 1998, *Phys. Rep.*, 302, 67

Lightman, A. P. 1974a, *ApJ*, 194, 419

Lightman, A. P. 1974b *ApJ*, 194, 419

Lovelace, R. V. E. 1976, *Nature*, 262, 649

Mahadevan, R., Narayan, R., & Krolik, J. 1997, *ApJ*, 486, 268

McConnell, M. et al. 1989, *ApJ*, 343, 317

McConnell, M. et al. 1994, *ApJ*, 424, 933

Meier, D. L., & Koide, S. 2000, private communications, at the Aspen Center for Physics

Meier, D. L., Koide, S., & Uchida, Y. 2001, *Science*, 291, 84

Miller, J. M. et al. 2001, *ApJ*, 546, 1055

Misner, C. W., Thorne, K. S., & Wheeler, J. A. 1973, *Gravitation* (New York: W. H. Freeman and Company)

Morgan, E. H., Remillard, R. A., & Greiner, J. 1997, *ApJ*, 482, 993

Novikov, I. D., & Thorne, K. S. 1973, in *Black Holes*, ed. C. DeWitt & B. S. DeWitt (New York: Gordon and Breach Science Publishers), 343

Penrose, R. 1969, *Rivista Del Nuovo Cimento: Numero Speciale*, 1, 252

Perlman, E. S., Sparks, W. B., Radomski, J., Packham, C., Fisher, R. S., Piña, R., & Biretta, J. A. 2001, *ApJ*, 561, L51

Piran, T., & Shaham, J. 1977, *Phys. Rev. D*, 16, No. 6, 1615

Piran, T., Shaham, J., & Katz, J. 1975, *ApJ*, 196, L107

Porcas, R. W. 1987, in *Superluminal Radio Sources*, ed. J. A. Zensus & T. J. Pearson (Cambridge: Cambridge Univ. Press), 12

Price, R. H. 1972, *Phys. Rev. D*, 5, 2419

Punsly, B. 1991, *ApJ*, 372, 424

Punsly, B., & Coroniti, F. V. 1989, *Phys. Rev. D*, 40, 3834

Remillard, R. A., Muno, M. P., McClintock, J. E., & Orosz, J. A. 2002, *ApJ*, 580, 1030 (astro-ph/0202305)

Shapiro, S. L., Lightman, A. P., & Eardley, D. M. 1976, *ApJ*, 204, 187

Stella, L., Vietri, M., & Morsink, S. M. 1999, 524, L63

Strohmayer, T. E. 2001, *ApJ*, 552, L49

Sturrock, P. A. 1971, *ApJ*, 164, 529

Sturrock, P. A., Petrosian, V., & Turk, J. S. 1975, *ApJ*, 196, 73

Thorne, K. S., Price, R. H., & Macdonald, D. A. 1986 *Black Holes: The Membrane Paradigm* (Yale University Press, New Haven)

Wagh, S. M., & Dadhich, N. 1989, *Phys. Rep.*, 183, 137

Wilkins, D. C. 1972, Phys. Rev. D, 5, 814

Williams, R. K. 1991, Ph.D. thesis, Indiana Univ.

Williams, R. K. 1995, Phys. Rev. D, 51, 5387

Williams, R. K. 1999, in Proceedings of The Eighth Marcel Grossmann Meeting on General Relativity, Jerusalem, Israel, ed. T. Piran & R. Ruffini (Singapore: World Science), 416

Williams, R. K. 2000, preprint

Williams, R. K. 2001, in Relativistic Astrophysics: 20th Texas Symposium, Austin, Texas, ed. J. C. Wheeler & H. Martel (New York: American Institute of Physics), 448 (astro-ph/0111161)

Williams, R. K. 2002a, ApJ, submitted (astro-ph/0306135)

Williams, R. K. 2002b, Phys. Rev. D, submitted (astro-ph/0203421)

Williams, R. K. 2003, ApJ, submitted

Williams, R. K., & Hjellming, R. M. (posthumous) 2002, to be submitted ApJ, in preparation

Wilms, J., Reynolds, C. S., Begelman, M. C., Reeves, J., Molendi, S., Staubert, R., & Kendziorra, E. 2001, MNRAS, 328, L27 (astro-ph/0110520)

Zhang, S. N., Cui, W., & Chen, W. 1997, ApJ, 482, L155

Zhang, W., Shrohmayer, T. E., & Swank, J. H. 1997, ApJ, 482, L167

Table 1: Model Parameters for 3C 273 (PCS)

Case no.	r (M)	E_e (MeV)	$\log(\nu_{\text{ph}})$ (Hz)	$\log(\nu_{\text{peak}})$ (Hz)	$\log(L_{\text{peak}})$ (erg/s)	$\log(L_{\text{obs}})$ (erg/s)	f_1	f_2
1 ^a	1.089	0.539 ^b	16.23	18.24	45.93	...	4.09 (−2)	1.0
2.....	1.099	0.456	17.09	18.91	46.20	46.0	4.17 (−2)	1.0 [0.632]
5.....	1.089	0.539 ^b	17.86	19.72	46.61	46.4	4.09 (−2)	1.0 [0.611]
6.....	1.089	0.539 ^b	18.86	20.21	46.27	...	4.09 (−2)	1.0
7.....	1.089	0.539 ^b	19.56	20.56	45.48	...	4.09 (−2)	1.0
8 ^c	1.089	1.435	18.86	20.61	47.12	46.2	4.09 (−2)	1.0 [0.121]
11.....	1.089	4.543	18.86	21.06	48.37	46.08	4.09 (−2)	1.0 [0.005]
13.....	1.089	11.79	18.86	21.46	49.34	46.08	4.09 (−2)	1.0 [0.001]

^aCase numbers 1 through 7 are for PCS by equatorially confined target electrons

^bWhen the more exact value is used for $r = r_{\text{mb}} = 1.091M$, $E_e \rightarrow 0.512 \text{ MeV} \simeq \mu_e$ (see Williams 1995, 2002a; Bardeen et al. 1972), as would be expected for equatorially confined orbits

^cCase numbers 8 through 13 are for PCS by nonequatorially confined target electrons

Table 2: Model Parameters for 3C 273 (PPP)

$r = r_{\text{ph}}$ Case no.	$(E_{\mp})_{\text{peak}}$ (MeV)	$\log(\nu_{\text{peak}})$ (Hz)	$\log(L_{\text{peak}})$ (erg/s)	$\log(L_{\text{obs}})$ (erg/s)	$f_1 = f_3$	$f_2 = f_4$	f_5
14 ^a	1.289	20.63	45.18	...	1.99 (-2)	1.0	1.0
15.....	6.626	21.21	46.32	46.06	1.99 (-2)	1.0 [0.8]	1.0 [0.859]
17.....	73.37	22.25	48.58	45.7	1.99 (-2)	1.0 [0.1]	1.0 [0.132]
19.....	174.6	22.59	49.36	45.6	1.99 (-2)	1.0 [0.05]	1.0 [0.069]
22.....	711.8	23.21	50.65	45.25	1.99 (-2)	1.0 [0.022]	1.0 [0.008]
25.....	2469	23.77	51.85	44.8	1.99 (-2)	1.0 [0.008]	1.0 [0.001]

^a Case numbers 14 through 25 have infalling initial (incident) photon frequency, used in the “secondary Penrose Compton scattering” (SPCS), $\nu_{\text{ph}} \simeq 7.24 \times 10^{18}$ Hz

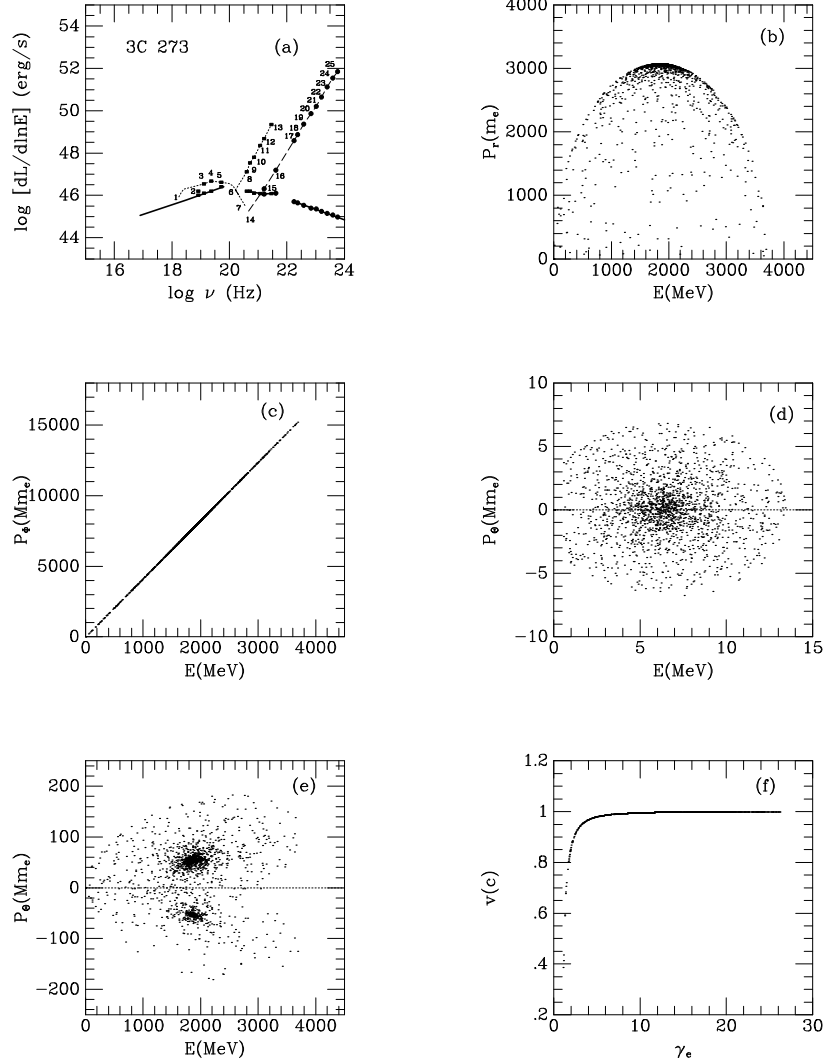


Fig. 1.— (a) Comparing the theoretical spectrum with observations for 3C 273. The calculated PCS and PPP ($\gamma\gamma \rightarrow e^-e^+$) luminosity spectra are represented by the solid squares and large solid dots, respectively. The observed spectra is indicated by the solid line. The upper curves with the solid squares and solid dots superimposed on the dotted line and the dashed line, respectively, for PCS and PPP ($\gamma\gamma \rightarrow e^-e^+$), are the spectra calculated from this model. Superimposed on the lower solid line of the observations are solid squares and solid dots that have been fitted to agree with observations. These fits depend on the f_n 's values (see text). (b) and (c) PPP ($\gamma\gamma \rightarrow e^-e^+$) at $r_{\text{ph}} = 1.074M$: scatter plots showing momentum components of the escaping e^-e^+ pairs (each point represents a scattering event). The radial momenta $(P_{\mp})_r$ vs. E_{\mp} , the azimuthal coordinate momenta $(P_{\mp})_{\Phi}$ ($\equiv L_{\mp}$) vs. E_{\mp} ; for the infalling photons $E_{\gamma 1} = 0.03$ MeV, and for the target photons $E_{\gamma 2} \simeq 3.893$ GeV, $(P_{\gamma 2})_{\Theta} = \pm 113 Mm_e$. (d) and (e) PPP ($\gamma\gamma \rightarrow e^-e^+$): polar coordinate momenta $(P_{\mp})_{\Theta}$ vs. E_{\mp} ; for $E_{\gamma 1} = 0.03$ MeV, $E_{\gamma 2} \simeq 13.54$ MeV, $(P_{\gamma 2})_{\Theta} = \pm 0.393 Mm_e$; and for $E_{\gamma 1} = 0.03$ MeV, $E_{\gamma 2} \simeq 3.893$ GeV, $(P_{\gamma 2})_{\Theta} = \pm 113 Mm_e$; respectively. (f) The velocity distribution vs. $\gamma_e (= E_{\mp}/m_e c^2)$ for the same case as (d) above. Note, $M = 10^8 M_{\odot}$.

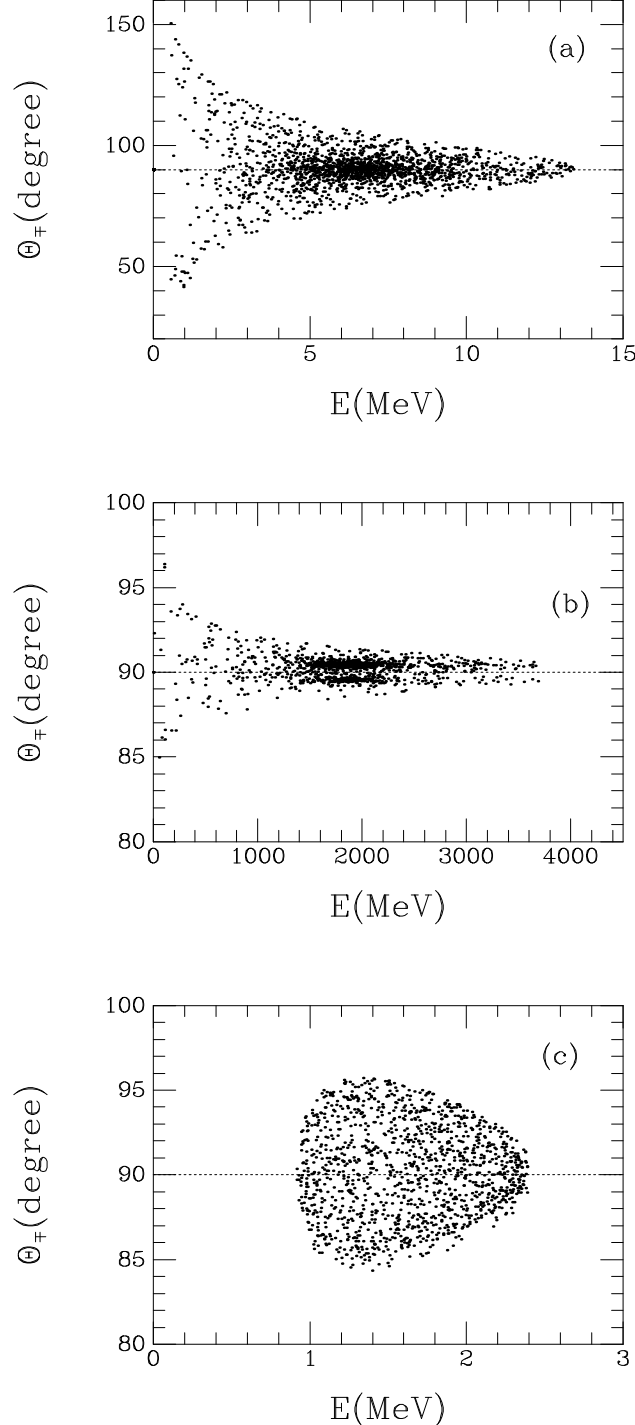


Fig. 2.— PPP ($\gamma\gamma \rightarrow e^-e^+$) at $r_{\text{ph}} = 1.074M$, for $M = 10^8 M_{\odot}$: scatter plots displaying polar angles, above and below the equatorial plane: Θ_{\mp} vs. E_{\mp} , of the escaping e^-e^+ pairs after 2000 event (each point represents a scattering event). The cases shown are defined by the following parameters: $E_{\gamma 1}$, the infalling photon energy; $E_{\gamma 2}$, the target photon orbital energy; $Q_{\gamma 2}^{1/2}$, corresponding polar coordinate momentum ($P_{\gamma 2}$)_Θ of the target photon; N_{es} , number of e^-e^+ pairs escaping. (a) $E_{\gamma 1} = 0.03$ MeV, $E_{\gamma 2} \simeq 13.54$ MeV, $Q_{\gamma 2}^{1/2} = \pm 0.393 Mm_e$, $N_{\text{es}} = 1850$. (b) $E_{\gamma 1} = 0.03$ MeV, $E_{\gamma 2} \simeq 3.893$ GeV, $Q_{\gamma 2}^{1/2} = \mp 113.0 Mm_e$, $N_{\text{es}} = 1997$. (c) $E_{\gamma 1} = 3.5$ keV, $E_{\gamma 2} \simeq 3.4$ MeV, $Q_{\gamma 2}^{1/2} = \mp 0.0987 Mm_e$, $N_{\text{es}} = 1326$. Note that, $\Theta_{\mp} > \pi/2$ is below the equatorial plane.

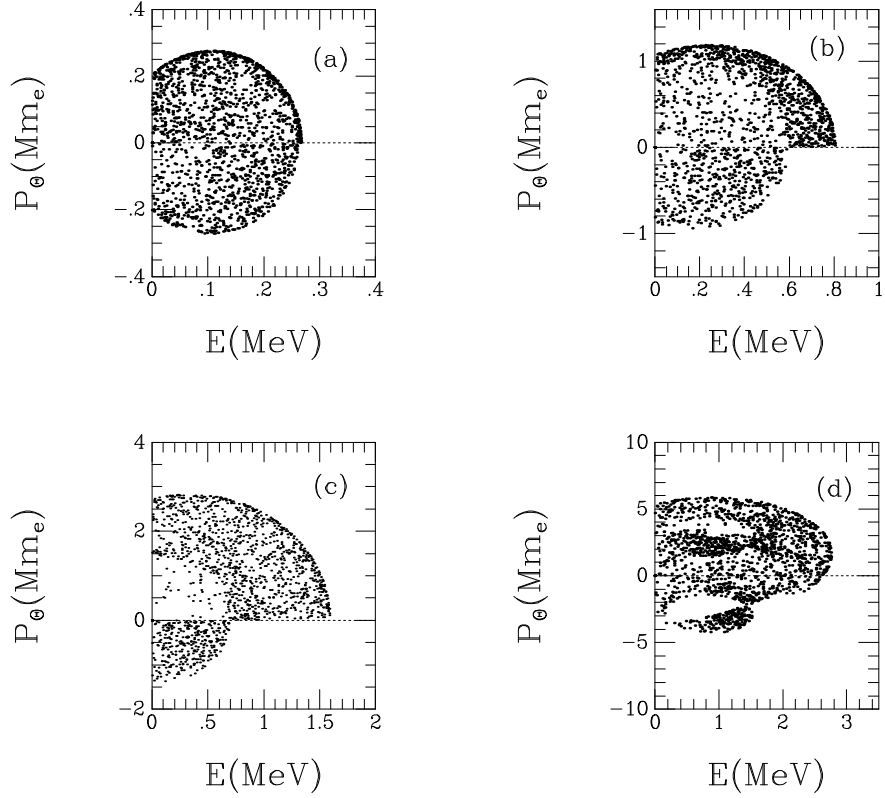


Fig. 3.— PCS: scatter plots showing polar coordinate space momenta: $(P'_{\text{ph}})_{\Theta} [\equiv (Q'_{\text{ph}})^{1/2}]$ vs. E'_{ph} , of the escaping PCS photons after 2000 events (each point represents a scattering event), at $r_{\text{mb}} \simeq 1.089M$, for $M = 10^8 M_{\odot}$. The various cases are defined by the following parameters: E_{ph} , initial photon energy; E_e , the target electron orbital energy; $Q_e^{1/2}$, defining the corresponding polar coordinate momentum $(P_e)_{\Theta}$ of the target electron; N_{es} , number of photons escaping. (a) $E_{\text{ph}} = 3.5$ keV, $E_e \simeq 0.539$ MeV, $Q_e^{1/2} = 0$, $N_{\text{es}} = 1637$. (b) $E_{\text{ph}} = 0.03$ MeV, $E_e \simeq 0.539$ MeV, $Q_e^{1/2} = 0$, $N_{\text{es}} = 1521$. (c) $E_{\text{ph}} = 0.15$ MeV, $E_e \simeq 0.539$ MeV, $Q_e^{1/2} = 0$, $N_{\text{es}} = 1442$. (d) $E_{\text{ph}} = 0.15$ MeV, $E_e \simeq 1.297$ MeV, $Q_e^{1/2} = \pm 2.479 Mm_e$, $N_{\text{es}} = 1628$. [Note, due to a minor oversight leading to improper treatment in the computer simulation of the arccosine term in eq. (3.39) of Williams (1995), correct Figs. 3a and 3b presented here replace Figs. 7(a) and 3(c), respectively, of Williams (1995).]

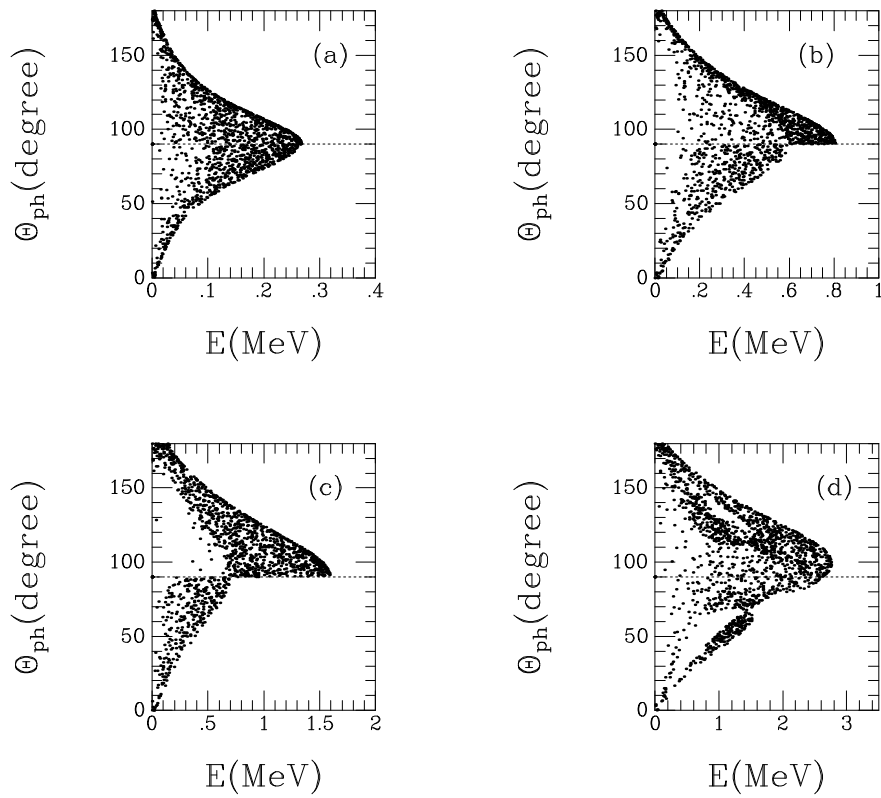


Fig. 4.— PCS: scatter plots displaying polar angles, above and below the equatorial plane: Θ'_{ph} vs. E'_{ph} , of the escaping PCS photons, for the cases 4a – 4d, described in Figs. 3a – 3d, respectively. Note that, $\Theta'_{\text{ph}} > \pi/2$ is below the equatorial plane.

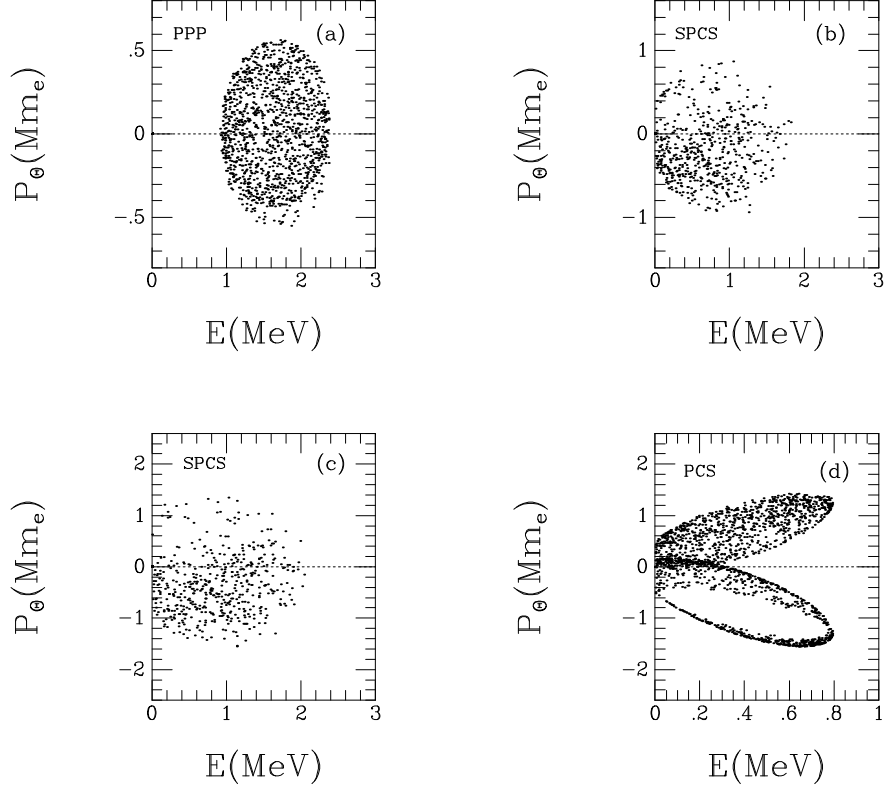


Fig. 5.— Self-consistent PPP ($\gamma\gamma \rightarrow e^-e^+$) and secondary Penrose Compton scattering (SPCS) at $r_{\text{ph}} = 1.074M$; and PCS by nonequatorially confined electron targets at $r_{\text{mb}} = 1.089M$; with $M = 30M_\odot$: scatter plots displaying the polar coordinate momenta, above and below the equatorial plane, versus the energy of the escaping particles, per 2000 infalling disk photons for each case shown (each point represents a scattering event). (a) PPP: $(P_\mp)_\Theta \equiv (Q_\mp)^{1/2}$ vs. E_\mp , with $E_{\gamma 1} = 3.5$ keV, $E_{\gamma 2} \simeq 3.4$ MeV, $Q_{\gamma 2}^{1/2} = \pm 0.125 Mm_e$; $\epsilon_\mp = 700/617$ (see text). (b) SPCS: $(P'_{\text{ph}})_\Theta \equiv (Q'_{\text{ph}})^{1/2}$ vs. E'_{ph} , with $E_{\text{ph}} = 3.5$ keV, see Fig. 5a for range of E_\mp and $Q_\mp^{1/2} \equiv (P_\mp)_\Theta$; $\epsilon_{\mp(\text{ph})} = 165/402$ (jet reversal; see text). (c) SPCS: $(P'_{\text{ph}})_\Theta$ vs. E'_{ph} , with $E_{\text{ph}} = 10$ keV, see Fig. 5a for range of E_\mp and $Q_\mp^{1/2} \equiv (P_\mp)_\Theta$; $\epsilon_{\mp(\text{ph})} = 127/363$ (jet reversal). (d) PCS: $(P'_{\text{ph}})_\Theta$ vs. E'_{ph} , with $E_{\text{ph}} = 3.5$ keV, $E_e \simeq 1.22$ MeV, $Q_e^{1/2} = \pm 2.3 Mm_e$; $\epsilon_{\text{ph}} = 1136/706$ (see text).

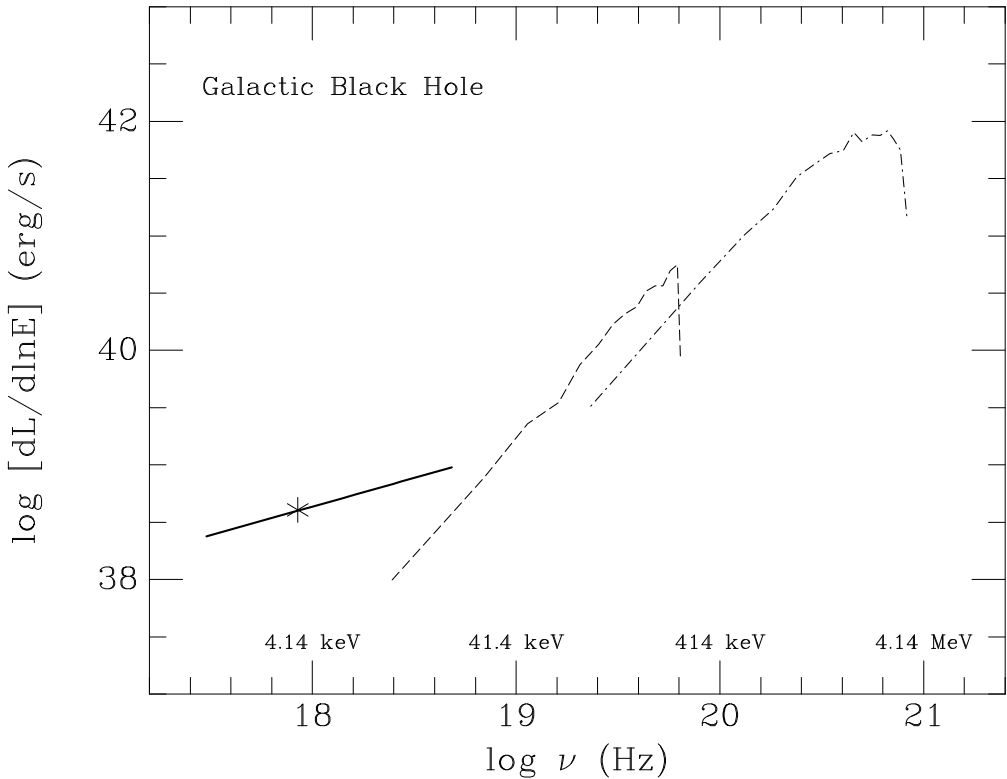


Fig. 6.— Self-consistent luminosity spectra of PCS by equatorially confined (dashed curve) electron targets at $r_{\text{mb}} = 1.089M$, and secondary Penrose Compton scattering (SPCS) by PPP electrons at $r_{\text{ph}} = 1.074M$ (dashed-dotted curve), with $M = 30M_{\odot}$. The total emitted spectrum is similarly to that observed for Cyg X-1 [$M \sim 10M_{\odot}$ (Liang 1998)]. The assumed power-law distribution accretion disk for the inner region ($K\nu^{-\alpha}$, where $\alpha = 1.5$), in the general range ($\sim 1.25 - 20$ keV), is shown (solid curve): the asterisk indicates monochromatic infalling photon energy producing the self-consistent Penrose processes displayed. For PCS by equatorially confined targets: $E_{\text{ph}} = 3.5$ keV, $E_e \simeq 0.539$ MeV, $Q_e = 0$. For SPCS by PPP electron targets: $E_{\gamma 1} = 3.5$ keV, $E_{\gamma 2} \simeq 5.012$ MeV, $Q_{\gamma 2}^{1/2} = \pm 0.185Mm_e$.